Cell dynamics underlying oriented growth of the *Drosophila* wing imaginal disc

Natalie A. Dye[1], Marko Popović[2], Stephanie Spannl[1], Raphaël Etournay[1,3], Dagmar Kainmüller[1,4], Eugene W. Myers[1,5], Frank Jülicher[2,5]* and Suzanne Eaton[1,6]*

*Corresponding authors

[1] Max Planck Institute of Molecular Cell Biology and Genetics

Pfotenhauerstrasse 108

01309 Dresden, Germany

[2] Max Planck Institute for the Physics of Complex Systems

Noethnitzer Strasse 38

01187 Dresden, Germany

[3] Unité de Génétique et Physiologie de l'Audition, Institut Pasteur

75015 Paris, France

4 Janelia Farm Research Campus

19700 Helix Dr

Ashburn, VA 20147, USA

[5] Center for Systems Biology Dresden

Pfotenhauerstrasse 108

01309 Dresden, Germany

[6] Biotechnologisches Zentrum

Technische Universität Dresden

Tatzberg 47/49

01309 Dresden, Germany

1   **ABSTRACT:**

2   Quantitative analysis of the dynamic cellular mechanisms shaping the *Drosophila* wing

3   during its larval growth phase has been limited, impeding our ability to understand how

4   morphogen patterns regulate tissue shape. Such analysis requires imaging explants under

5   conditions that maintain both growth and patterning, as well as methods to quantify how much

6   cellular behaviors change tissue shape. Here, we demonstrate a key requirement for the steroid

7   hormone 20-hydroxyecdysone (20E) in the maintenance of numerous patterning systems *in*

8   *vivo* and in explant culture. We find that low concentrations of 20E support prolonged

9   proliferation in explanted wing discs in the absence of insulin, incidentally providing novel

10   insight into the hormonal regulation of imaginal growth. We use 20E-containing media to

11   directly observe growth and apply recently developed methods for quantitatively decomposing

12   tissue shape changes into cellular contributions. We discover that while cell divisions drive

13   tissue expansion along one axis, their contribution to expansion along the orthogonal axis is

14   cancelled by cell rearrangements and cell shape changes. This finding raises the possibility that

15   anisotropic mechanical constraints contribute to growth orientation in the wing disc.

16

INTRODUCTION:

The *Drosophila* larval wing imaginal disc is a powerful model system in which to study the integration of diverse types of regulatory cues for tissue growth. The wing disc is a relatively flat epithelial sac that grows to about 50,000 cells during larval stages of development. As it grows, the rapidly proliferating cells on one side (the wing pouch) become pseudostratified, while cells on the other side become squamous. At pupariation, the wing pouch everts and flattens to assume the adult wing shape (Waddington 1940).

The size and shape of the wing are largely, but not entirely, determined during the larval growth phase. At this stage, signaling centers located at the anterior-posterior (AP) and dorsal-ventral (DV) compartment boundaries not only establish patterns of gene expression but also promote growth (Beira & Paro 2016; Hartl & Scott 2014). Hedgehog produced in posterior cells signals across the AP boundary to stabilize the transcriptional activator Ci155 and induce the expression of different target genes (i.e., Engrailed and Decapentaplegic (Dpp)) at different distances (reviewed in (Hartl & Scott 2014)). Dpp is itself a secreted signaling molecule that establishes a bidirectional gradient anteriorly and posteriorly, promoting patterned gene expression through graded phosphorylation of SMAD transcription factors (reviewed in (Affolter & Basler 2007)). At the DV boundary, Wingless (Wg) expression and Notch signaling are maintained by a positive feedback loop and together pattern the DV axis (Micchelli & Blair 1999; Micchelli et al. 1997; Rulifson et al. 1996). Signaling from the AP and DV organizers is required for wing disc growth, even though cell proliferation is not especially concentrated near these regions (Schwank et al. 2011; González-Gaitán et al. 1994; Milán et al. 1996).

The orientation of tissue growth is strikingly non-uniform: marked clones strongly elongate along the proximo-distal (PD) axis of the adult wing (González-Gaitán et al. 1994; Resino et al. 2002; Baena-López et al. 2005; Mao et al. 2013; Worley et al. 2013; Heemskerk et al. 2014). In central regions of the larval wing pouch, the adult PD axis is generally orthogonal to the DV boundary. Signaling at organizer regions influences the growth orientation by establishing tissue-wide patterns of two planar cell polarity (PCP) systems, Fat and Core, with distinct cortical complexes that are polarized in the epithelial plane (Aw & Devenport 2016). Both systems develop the same global pattern of planar polarity, which is oriented with respect to the AP and DV boundaries and presages the orientation of growth (Rogulja et al. 2008; Ambegaonkar et al. 2012; Sagner et al. 2012; Brittle et al. 2012). Perturbing Fat PCP or dominantly reversing the orientation of Core PCP both disrupt wing size and shorten it in the PD axis (Bryant et al. 1988; Clark et al. 1995; Mao et al. 2006; Merkel et al. 2014).

50   A complete description of how the PCP patterns direct oriented tissue growth is still

51   missing. PD-oriented cell divisions clearly contribute to oriented tissue growth and are

52   disturbed by genetic disruption of the Fat pathway (Baena-López et al. 2005; Mao et al. 2011).

53   However, quantitatively, it is still unknown the extent to which oriented cell divisions or other

54   dynamic behaviors (T1 rearrangements, cell shape changes or extrusions) determine the tissue

55   growth pattern. Analytical tools now exist to fully describe tissue growth from cellular dynamics

56   (Merkel et al. 2017; Etournay et al. 2015; Etournay et al. 2016; Guirao et al. 2015), but such

57   analysis demands long-term time-lapse imaging at high spatial and temporal resolution. *In vivo*

58   imaging has an insufficient time resolution (Heemskerk et al. 2014), necessitating the use of *ex*

59   *vivo* culture. The achievement of prolonged *ex vivo* wing disc growth has proven difficult, even

60   though the dramatic eversion process that imaginal tissues undergo at the onset of pupariation

61   can be successfully replicated in culture (Fristrom et al. 1973; Milner 1977; Aldaz et al. 2010).

62   Importantly, in order to properly study the cellular dynamics underlying oriented growth, we

63   require a culture condition that maintains the signaling from AP/DV organizers and global PCP

64   patterns, and the consequences for culture on these systems is completely unknown.

65   Insulin signaling regulates animal size in response to nutrition, and bovine insulin has

66   been widely used in culture to stimulate growth of explanted discs (Zartman et al. 2013; Mao et

67   al. 2011; Mao et al. 2013; Legoff et al. 2013; Heller et al. 2016; Tsao et al. 2016). However,

68   proliferation in insulin-cultured discs arrests within a few hours (Handke et al. 2014; Tsao et al.

69   2016); thus clearly other signals are required for long term growth. One such missing signal

70   could be ecdysteroids, a family of steroid hormones produced by the ring gland in arthropods

71   with well characterized functions in regulating major developmental transitions (Kozlova &

72   Thummel 2000). A peak of 20-hydroxyecdysone (20E) and related hormones at the larval to

73   pupal transition induces pupariation and imaginal disc eversion (Fristrom et al. 1973; Milner

74   1977; Aldaz et al. 2010). This peak is preceded by a smaller elevation in hormone levels

75   (approximately 25-fold lower concentration) that starts in the mid-third larval instar (Kozlova &

76   Thummel 2000; Lavrynenko et al. 2015). Several lines of evidence now suggest that these lower

77   concentrations promote imaginal growth and development during larval stages (Bodenstein

78   1943; Brennan et al. 1998; Brennan et al. 2001; Mirth et al. 2009; Delanoue et al. 2010; Mitchell

79   et al. 2013; Herboso et al. 2015).

80   Here, we show that physiologically low levels of 20E, in the absence of insulin,

81   significantly extend the proliferation of explanted wing discs over insulin alone. Furthermore,

82   we show with transcriptome sequencing that 20E is required in culture for the normal

83   expression of numerous genes involved in wing patterning, whereas insulin promotes a strong

84   but transient anabolic growth response. Genetic perturbations *in vivo* confirm that 20E has

4

85   widespread effects on morphogen signaling and PCP in the larval wing, highlighting the

86   importance of including 20E in culture media for replicating *in vivo* growth patterns. We exploit

87   this improved system to perform live imaging and apply recent tools for decomposing tissue

88   growth into contributions from each type of dynamic cell behavior (Merkel et al. 2017; Etournay

89   et al. 2015; Etournay et al. 2016). Our analysis indicates that divisions alone are insufficient to

90   quantitatively account for the anisotropy of tissue growth, as previously thought; cell

91   rearrangements and cell shape changes play an equally important role. This work inspires new

92   directions for exploration into the regulation of tissue size and shape in this system.

93   **RESULTS:**

94   **Low levels of 20E stimulate cell divisions in cultured wing discs**

95   We directly tested the ability of low levels of 20E, with or without insulin, to maintain

96   proliferation in explants from mid third instar larvae (96hr after egg laying (AEL)) grown at 25

97   °C. These discs should continue to proliferate for another 24hr *in vivo*, since under the

98   conditions we use, pupariation occurs around 120hr AEL.

99   We monitored the numbers of phospho-histone H3-positive proliferating cells in freshly

100   explanted discs, and compared them to discs cultured in the absence of hormones, or in the

101   presence of 20nM 20E, 1μM insulin, or both hormones (Fig. 1A,B). In the absence of any

102   hormones, the number of mitotic cells per area (proliferation index) is dramatically reduced by

103   4hr and negligible by 9hr (Fig. 1Ai, Bi), consistent with previous work (Zartman et al. 2013;

104   Handke et al. 2014). In insulin, the proliferation index drops to half that of freshly explanted

105   discs after 4hr and continues to decline thereafter (Fig. 1Aii, Bii). These indices quantitatively

106   agree with those of previous analyses of insulin-culture discs (Handke et al. 2014).

107   Strikingly, in 20E alone, the proliferation index is similar to that of insulin-cultured discs

108   at 4hr, but instead of declining thereafter, the index actually increases (Fig. 1Aiii, Biii). From 9-

109   16hr after explant, the same density of mitotic nuclei is found in 20E-cultured discs as in freshly

110   explanted discs. Proliferation even extends through 24hr, albeit at a lower density than between

111   9-16hr. By 24hr, the overall morphology also becomes somewhat abnormal (Fig. 1—Figure

112   Supplement 1), perhaps reflecting the fact that components of the extracellular matrix come

113   from the fat body *in vivo* (Pastor-Pareja & Xu 2011)*.*

114   The simultaneous addition of both hormones promotes proliferation mildly better than

115   either alone for 4hr; but by 9hr, proliferation declines, and the cell area distribution becomes

116   abnormal (Fig. 1B-C). Growth is not significantly improved by adjusting 20E concentration (Fig.

117   1-Figure Supplement 1). Thus, under these explant conditions, insulin antagonizes the effect of

118   20E on proliferation.

119   **Transcriptional responses to 20E and insulin in explanted wing discs**

120   To assess the consequences for gene expression of culturing under different hormonal

121   conditions, we sequenced the transcriptomes from freshly explanted discs, discs cultured

122   without hormones for 4hr, and discs cultured for 4 or 9hr in either 20E or insulin alone. Relative

123   to freshly explanted discs, the expression of 1604 genes goes down and 1409 genes goes up

124   after 4hr of culture without hormones. Changed expression of 1911 genes (63%) could be

6

125   prevented, at least transiently, by the addition of either 20E or insulin. While some genes

126   responded to both 20E and insulin, others were hormone-specific.

127   Figure 2 shows the size and overlap of the hormone-responsive gene sets. Comparing

128   the transcriptional response to insulin at 4 and 9hr reveals that it is largely transient (Fig. 2A),

129   consistent with the decreased proliferative response to insulin by 9hr (Fig. 1Aii,Bii). In contrast,

130   although 20E regulates a smaller subset of genes, its effects are longer lasting (Fig. 2A).

131   Interestingly, a subset of genes can be regulated by either 20E or insulin (Fig. 2B). Maximum

132   overlap (353 genes) occurs at time points when each hormone supports maximum proliferation

133   (insulin at 4hr, 20E at 9hr).

134   Insulin-induced genes are most significantly enriched in Gene Ontology (GO) terms

135   describing DNA replication, ribosome biogenesis, translation, purine biosynthesis, and

136   mitochondrial biogenesis (Fig. 3 and Fig. 3-Figure Supplement 1). Conversely, insulin reduces

137   the expression of genes involved in autophagy and cell death (Fig. 3 and Fig. 3-Figure

138   Supplement 1). Interestingly, the effect of insulin on genes in all of these GO categories is much

139   stronger at 4hr than at 9hr of culture. This transient response to insulin must result from

140   negative regulation of the pathway downstream of PI3K: a reporter of PI3K activation remains

141   active even after 9hr of culture (Fig. 3-Figure Supplement 2). Thus, insulin induces a pattern of

142   gene expression characteristic of the fed state, consistent with many previous studies

143   (Gershman et al. 2007; Teleman et al. 2008; Li et al. 2010); however, this response is transient.

144   Between the insulin and 20E-responsive gene sets, there is limited overlap of enriched

145   GO terms (Fig. 4 and Fig. 4-Figure Supplement 1). Both hormones repress genes involved in

146   autophagy, DNA damage response and cell death while inducing genes involved in DNA

147   replication. Amongst the shared targets, we found a subset involved in protein synthesis and

148   nutrient transport (Fig. 4-Figure Supplement 1C). These include 4E-BP, which was previously

149   shown to respond to 20E *in vivo* (Herboso et al. 2015).

150   Unlike in the insulin targets, significantly enriched GO terms in the 20E-induced genes

151   describe a variety of developmental processes (Fig. 4). Genes with these GO terms include

152   components and targets of the Notch, Wg, EGF, and JAK/STAT pathways (Fig. 5). Also

153   significantly affected was *sugarless,* which is required to synthesize the heparan sulfate moieties

154   of proteoglycans needed for Dpp, Hh, FGF and Wg signaling (Hacker et al. 1997; Bornemann et

155   al. 2004; Yan & Lin 2009). 20E, and not insulin, also supports the expression of a wide variety of

156   developmentally important transcription factors, chromatin modifying proteins, and many

157   genes that regulate tissue morphogenesis, including junctional, cytoskeletal and ECM

158   components (Fig. 5). A smaller set of developmentally important genes seems to be regulated by

7

159   either hormone; however 20E generally causes a more potent and long-lasting response in this

160   group (Fig. 4 – Figure Supplement 1C). Of the genes that only 20E induces, roughly 30% are

161   already known to perturb wing development when mutated.

162   On the whole, these transcriptional data suggest that insulin promotes proliferation

163   through its well-understood effects on anabolic metabolism. However, 20E promotes

164   proliferation over longer times while influencing only a subset of the direct growth promoting

165   genes activated by insulin. Instead, 20E supports the expression of genes involved in wing

166   patterning and morphogenesis.

167   **Perturbation of 20E signaling disrupts wing disc patterning *in vivo***

168   To determine whether our data from explant culture reflect an *in vivo* requirement for

169   20E in maintaining patterning systems during growth, we genetically perturbed 20E signaling *in*

170   *vivo* and then assessed its effect on a broad range of morphogen and PCP pathways (Fig. 6). To

171   do this, we expressed a dominant negative Ecdysone receptor (EcR-DN) in the dorsal

172   compartment of wing imaginal discs for 24hr of the third larval instar. Consistent with previous

173   results (Herboso et al. 2015), EcR-DN expression autonomously reduces tissue size and the

174   number of mitotic cells (Fig. 6-Figure Supplement 1A). However, the tissue appears otherwise

175   healthy – caspase staining reveals no elevation in apoptosis ((Herboso et al. 2015) and data not

176   shown), and neither localization nor protein levels of Discs large is perturbed (Fig. 6A).

177   Expressing EcR-DN in the dorsal compartment decreases Wg expression both in the

178   hinge and in the stripe at the DV boundary (Fig. 6Bi). The autonomous effect of EcR-DN on the

179   DV boundary Wg stripe is more obvious when it is expressed only in the posterior compartment

180   (Fig. 6-Figure Supplement 2). The effect of EcR-DN expression clearly reflects a true

181   requirement for 20E, as wing discs deprived of 20E *in vivo* have severely reduced levels of Wg

182   and also less growth (Fig. 6—Figure Supplements 1B and 3A). These results are consistent with

183   previously published data showing that EcR-DN expression can block Wg expression (Mirth et

184   al. 2009; Herboso et al. 2015).

185   In wild type discs, both E-Cadherin and Delta are upregulated by Wg signaling on either

186   side of the DV boundary (Micchelli et al. 1997; Jaiswal et al. 2006; de Celis & Bray 1997). Dorsal

187   EcR-DN expression prevents both from accumulating on the dorsal side of the DV boundary,

188   consistent with reduced Wg signaling there (Fig. 6Bii-iii). Like at the DV boundary, EcR-DN

189   expression also affects elevated Delta expression on either side of a region of high Hedgehog

190   signaling near the AP boundary (Fig. 6Bii). This effect on Delta is consistent with our

191   transcriptomic data showing that mRNA levels of Delta itself, as well as effectors of the EGF and

192   Notch pathways that regulate the AP Delta pattern, drop in culture without 20E (Fig 5).

193   Also consistent with our transcriptomic data, we found that Dally-like protein levels are

194   considerably reduced in the EcR-DN expressing compartment (Fig. 6Biv). Given the broad

195   effects of HSPG on morphogen signaling, we therefore also looked at Hh and Dpp pathway.

196   Indeed, EcR-DN decreases levels of pMAD (a readout of Dpp signaling) in the posterior

197   compartment (Fig. 6Ci). Furthermore, Hh protein levels and signaling are strongly affected (Fig.

198   6Cii-iv). Hh staining intensity decreases in the posterior producing cells, consistent with roles

199   for Dally and Dally-like in controlling its trafficking there (Ayers et al. 2010; Ayers et al. 2012;

200   Eugster et al. 2007). Furthermore, the gradient in the anterior receiving cells is diminished and

201   the amplitude and range of Hedgehog signaling outputs are reduced. Ci is stabilized over a

202   shorter distance from the AP boundary (Fig. 6Ciii). Engrailed expression is also reduced– both

203   anterior to the AP boundary, where expression is activated by Hh signaling, and posteriorly

204   where its expression is maintained independently of Hh by chromatin modifications (DeVido et

205   al. 2008) (Fig. 6Civ). The Hh gradient and signaling output was severely reduced in wing discs

206   from larvae deprived of 20E *in vivo*, confirming that the effects of EcR-DN expression reflect a

207   real requirement for 20E (Fig. 6-Figure Supplement 3B-D).

208   Our transcriptomic analysis also revealed that 20E affects expression of the Core PCP

209   component Prickle and the Fat PCP component Four-jointed (Fig. 5, Fig. 4-Figure Supplement 1).

210   To examine global patterns of PCP upon EcR-DN expression, we stained discs with antibodies to

211   Dachsous (Ds) and Flamingo (Fmi). Neither of these proteins was transcriptionally affected by

212   20E in culture, but their patterns of subcellular localization should reveal any disturbances in

213   global PCP patterns. Strikingly, EcR-DN expression dramatically lowered protein levels of both

214   Ds and Fmi, presumably post-transcriptionally, such that any residual planar polarity was

215   unquantifiable (Fig. 6D).

216   In summary, both *in vivo* experiments and transcriptomic data from explanted discs

217   suggest that 20E is required to maintain the signal transduction and planar cell polarity

218   pathways that drive growth and patterning in the wing imaginal disc. Given its key role of

219   regulating patterning *in vivo* and *in vitro*, addition of 20E to explant culture should be critical for

220   measuring normal patterning of growth.

221   **Cellular contributions to oriented tissue growth**

222   Having established that 20E supports longer proliferation and is better than insulin at

223   maintaining the gene expression patterns underlying oriented growth, we used the new 20E-

224   containing media to investigate the cell dynamics underlying growth and its anisotropy with

225   live imaging. We analyzed three discs in 13hr timelapses.

226   We first examined area change in the wing pouch and its cellular contributions (Fig.

227   7Bi). We note that tissue area (blue line in Fig. 7Bi) decreases during the first two hours, almost

228   entirely as a consequence of cell area changes (green line in Fig. 7Bi), suggesting that some time

229   is required for discs to adapt to culture or recover from mounting. However, after the

230   adaptation phase, tissue area grows. Cell divisions contribute positively to tissue area growth

231   and are only partly counteracted by modest levels of cell extrusion (cyan line in Fig. 7Bi) and

232   slight cell area reduction (Fig. 7Bi). This slight reduction in cell area is consistent with *in vivo*

233   observations of growth over development time (Aegerter-Wilmsen et al. 2012; Mao et al. 2013).

234   To analyze the anisotropy of tissue growth in 20E, we measured the patterns of pure

235   tissue shear accumulated during 11hr after the 2hr adaptation phase using the Tissue Miner

236   computational framework (Etournay et al. 2016) and Triangle Method (Merkel et al. 2017)

237   described previously. Pure shear describes a change in aspect ratio irrespective of area change.

238   In Fig. 7A, local cumulative tissue shear is indicated by a line whose length is proportional to the

239   magnitude of pure shear and whose orientation indicates its axis. We observe that tissue shear

240   is oriented perpendicular to an axis defined by the DV boundary throughout the tracked region

241   of the wing pouch, generally consistent with analyses of *in vivo* clone data (González-Gaitán et

242   al. 1994; Resino et al. 2002; Baena-López et al. 2005; Worley et al. 2013; Mao et al. 2013;

243   Heemskerk et al. 2014).

244   To examine the dynamics of tissue shape change, and its underlying cellular

245   contributions, we accumulated the average tissue shear and its cellular contributions over the

246   entire tracked region using a coordinate system with an x-axis corresponding to the DV

247   boundary (dashed horizontal line in Fig. 7A) and a y-axis perpendicular to it. In this coordinate

248   system, a positive xx component of shear corresponds to shear parallel to the DV boundary,

249   while a negative xx component of shear corresponds to shear perpendicular to the DV

250   boundary. Fig. 7Bii (blue line) shows the average xx component of tissue shear throughout the

251   tracked region, accumulated over time after the adaptation phase. These plots reveal that the

252   wing pouch becomes more anisotropic as it grows. Examining the cellular contributions to

253   tissue shear reveals that cell divisions (orange line in Fig. 7Bii) contribute to the change in shape

254   of the wing pouch during growth. However, cell division orientation cannot entirely account for

255   tissue shear: quantitatively similar contributions to tissue shear stem from both cell

256   rearrangements (red line in Fig. 7Bii) and cell shape changes (green line in Fig. 7Bii).

257   Comparing the outlines of the wing pouch at the beginning and end of the movies (Fig.

258   7A) suggests that wing pouch tissue is expanding almost entirely perpendicular to the DV

259   boundary. To separately quantify expansion along the x- and y-axes over time, we determined

260   the xx and yy components of velocity gradient tensor based on the measured shear and area

261   expansion (see Methods). Indeed, tissue expansion (blue lines in 7Biii and 7Biv) occurs along

262   the y-axis, perpendicular to the DV boundary (Fig. 7Biv) and not along the x-axis (Fig. 7Biii). We

263   decomposed the xx and yy components of the tissue velocity gradient tensor into their

264   respective cellular contributions (see Methods). This calculation reveals that expansion of the

265   wing pouch along the y-axis is almost identical to the expansion contributed by cell divisions in

266   all three movies (compare orange and blue lines in Fig. 7Biv). Surprisingly, along the x-axis, the

267   relationship between tissue flow and cell divisions is very different. Expansion due to cell

268   divisions is only slightly smaller along the x-axis than along the y-axis (orange lines in Fig. 7Biii-

269   iv). Nevertheless, the xx component of tissue velocity gradient is small and negative – i.e. the

270   tissue does not expand in this axis but rather contracts slightly. In this direction, the sum of the

271   other cellular contributions is larger than along the y-axis and balances the contribution from

272   cell divisions. We note that although the contributions of cell shape changes, rearrangements

273   and extrusions vary in each of the three movies, they always combine to cancel the expansion

274   along the x-axis due to cell division.

275   In summary, we use the improved method for long-term cultivation of wing imaginal

276   discs to directly measure the cellular contributions to tissue shape and area changes. This

277   analysis revealed that contributions from cell divisions to tissue shape changes are not nearly as

278   anisotropic as tissue flow and indicates that additional morphogenetic mechanisms exist to

279   prevent expansion of the wing parallel to the DV boundary.

DISCUSSION:

This work considerably expands our understanding of the cell dynamics in the growing *Drosophila* wing disc, revealing important contributions from cell rearrangements and cell shape changes to oriented tissue growth. Our analysis provides the foundation for future experiments aimed at understanding how patterned gene expression and tissue mechanics regulate cellular behavior during tissue growth. Furthermore, our transcriptomic data from wing discs cultured in 20E or insulin provide a novel global view of the direct response of wing imaginal tissues to these hormones. These data have *in vivo* implications for the organismal coordination of growth and development and constitute a valuable resource for the planning of any type of experiment requiring wing disc culture.

20E supports normal growth of cultured wing discs, independently of insulin

Studying the cellular basis of tissue development requires prolonged, high time resolution imaging that is ideally entirely *in vivo*. However, the *Drosophila* wing grows during larval stages, when animals are mobile and feeding, and thus a completely *in vivo* approach to imaging growth is practically not feasible. While advances in clonal marking and imaging methods now allow the periodic monitoring of clone size and shape in the same animal over its development (Heemskerk et al. 2014), the available frame rate is still far too low to study cell dynamics. Analyzing whether cell boundary exchanges that are noisy and dynamic have an orientation, for example, demands the integration of high time resolution data over as much time as possible. Explant culture is the only option, provided that the patterning systems that drive oriented growth can be maintained.

While previous studies have used insulin to sustain discs long term in culture (Zartman et al. 2013; Mao et al. 2011; Mao et al. 2013; Legoff et al. 2013; Handke et al. 2014; Heller et al. 2016; Tsao et al. 2016), we show that the expression of numerous genes involved in patterning declines when discs are cultured without the steroid hormone 20E. 20E was previously thought to promote imaginal growth by repressing the expression of the translational inhibitor 4E-BP (Herboso et al. 2015); however, we show here that in addition, 20E broadly affects many different signaling pathways, each one of which is critical for growth. These data indicate that the inclusion of 20E in culture media should be critically important to the goal of replicating *in vivo* growth patterns. While high concentrations of 20E promote eversion, 10-fold lower concentrations promote growth in the absence of insulin. This condition actually supports proliferation for longer than insulin-containing media: up to ~24hrs in 20E, compared to only ~7-10hrs in insulin (Fig. 1, and (Zartman et al. 2013; Handke et al. 2014; Tsao et al. 2016)).

313   How does the growth of 20E-cultured discs compare to that *in vivo*? Although discs can

314   proliferate in culture up to 24hr, they slow down sooner (after ~13hr) if they are continuously

315   imaged. Nonetheless, for the first 13hr of live imaging, our direct quantification of the pattern of

316   tissue growth agrees well with data generated using indirect methods to follow growth *in vivo*

317   (González-Gaitán et al. 1994; Resino et al. 2002; Baena-López et al. 2005; Mao et al. 2013;

318   Worley et al. 2013; Heemskerk et al. 2014). We also confirm the data from fixed tissues (Baena-

319   López et al. 2005) showing that cell divisions are slightly biased to be perpendicular to the DV

320   boundary, at least in central regions of the pouch (compare orange lines in Fig. 7Biii-iv). We

321   estimate that the overall cell doubling time in continuously imaged explanted discs is about 3x

322   longer than the estimated rate in well-fed animals (Garcia-Bellido & Merriam 1971; Bryant &

323   Levinson 1985; González-Gaitán et al. 1994; Heemskerk et al. 2014). However, phototoxicity

324   associated with continuous imaging seems to affect not just the duration but also the rate of

325   proliferation: estimating the rate from the density of PH3-stained nuclei in discs that were not

326   continuously imaged suggests a value that is closer to that of freshly explanted discs (Fig. 1).

327   Interestingly, *in vivo*, if animals are starved after the attainment of a critical weight, the

328   release of insulin-like peptides from the brain is reduced (Géminard et al. 2009) and growth

329   arrests in the larval – but not imaginal – tissues (Britton & Edgar 1998; Cheng et al. 2011). The

330   rate of imaginal proliferation during this so-called "sparing" condition is ~60% lower than in

331   the well-fed state (Cheng et al. 2011). Thus, proliferation of explants given 20E but not insulin

332   may be closer to this *in vivo* low-insulin state. Importantly, while the ablation of insulin-

333   producing cells in the brain reduces the size of the emerging adult wings, these wings are

334   nevertheless well-proportioned (Rulifson et al. 2002). Thus, the orientation of tissue growth

335   and its underlying cell dynamics is likely to be preserved in discs cultured with 20E in the

336   absence of insulin. Perhaps the slight but reproducible lag in the division rate at early times of

337   20E culture (Fig. 1Biii and Fig. 7Bi) reflects a transition phase when discs taken from well-fed

338   animals must switch to an insulin-independent/20E-dependent mode of growth.

Implications for hormonal regulation of growth

340   The mechanism underlying the sparing of imaginal tissues is unknown. Sparing of the

341   central nervous system involves a locally provided ligand that activates downstream signaling

342   in the insulin pathway (Cheng et al. 2011). Our transcriptomic data provide no evidence that

343   wing discs can produce their own insulin-like ligands or that they activate insulin signaling in

344   the absence of exogenous ligands. Nonetheless, wing discs in culture continue to proliferate in

345   20E, even when no insulin-like ligand is present. This finding raises the possibility that 20E is

346   also sufficient to support their proliferation *in vivo* during starvation. While 20E promotes

347   imaginal growth, it inhibits that of larval tissues (Delanoue et al. 2010), potentially explaining

348   the opposite response to starvation of these two tissue types.

349   Under well-fed conditions, insulin signaling must be able to combine with 20E signaling

350   to further increase imaginal disc growth, but this feature is not reproduced in culture (Fig. 1Biv)

351   and (Handke et al. 2014). *Drosophila* has 7 Insulin-like peptides that interact not only with the

352   single receptor, but also with other proteins that modulate their activities (Honegger et al. 2008;

353   Arquier et al. 2008; Okamoto et al. 2013). Perhaps specific insulin peptides or their binding

354   proteins allow proper interfacing with 20E signaling to promote growth.

355   **Cellular dynamics underlying oriented tissue growth in the wing disc**

356   While the mechanisms dictating cell division orientation in this tissue have been studied

357   (Mao et al. 2011; Mao et al. 2013; Legoff et al. 2013), it has remained unclear to what extent the

358   observed slight bias in cell division orientation could account for the orientation of tissue

359   growth. Is cell division the only behavior that contributes to oriented tissue growth? The

360   Triangle Method (Merkel et al. 2017; Etournay et al. 2015) for decomposing tissue shape

361   changes into quantitative contributions from all types of cellular events provides the

362   measurement tool to connect the cell and tissue scales. Our results reveal that the observed bias

363   in cell division orientation in the central region of the disc is insufficient to explain the

364   anisotropy of tissue growth. While expansion of the tissue perpendicular to the DV axis is driven

365   primarily by cell divisions, in the orthogonal direction, cell shape changes and T1 transitions

366   fully cancel the contribution to expansion by cell divisions, such that the wing does not expand

367   along an axis parallel to the DV boundary.

368   Previous efforts to quantify cell rearrangements have used live imaging of discs cultured

369   in insulin and have concluded that they occur either with very low frequency (Gibson et al.

370   2006; Legoff et al. 2013), or with a significant frequency but no pattern or orientation at the

371   tissue-scale (Mao et al. 2013; Heller et al. 2016). In contrast, we see that the contribution of cell

372   rearrangements to tissue growth is quantitatively similar to that of oriented cell division and

373   helps restrict growth parallel to the DV boundary. This discrepancy could either come from the

374   differing culture conditions (lack or presence of 20E) or to the inherent difficulties in defining

375   and counting cell rearrangements. A classic T1 transition occurs when two pairs of cells

376   exchange neighborships: the connecting bond between two cells shrinks as all cells come

377   together to make a 4-way vertex; then, a new bond is formed such that the two cells that were

378   originally separated come into contact, while the two that were originally together stay

379   separate. But sometimes the 4-way vertex simply resolves back without changing the original

380   neighborship, and sometimes the neighborship fluctuates back and forth several times. How and

381   when do you count the rearrangement? The method that we use overcomes the problem of

382   having to classify a "true" T1 event based on observation time windows. It considers all changes

383   in neighborship, regardless of the length of time they persist, and quantifies their accumulated

384   contribution to tissue shape change. Note that the shear decomposition method we use does not

385   simply quantify the number and orientation of T1s but the tissue shape change that they cause.

386   This approach may be key to our ability to detect and quantify the important contribution of cell

387   rearrangements to oriented growth of the wing disc.

388   What mechanisms might allow cell rearrangements, cell shape changes and cell

389   extrusions to cancel expansion due to cell division specifically in one direction? We propose that

390   a mechanical constraint prevents wing pouch expansion parallel, but not perpendicular, to the

391   DV boundary. In this case, area growth due to cell division would lead to anisotropic expansion

392   with corresponding anisotropic stresses that could be associated with oriented cell shape

393   changes and rearrangements. Consistent with this idea, we observe that the sum of expansion

394   due to rearrangements, shape changes and extrusions is more reproducible than their

395   individual cellular contributions. Long range anisotropic stresses could coordinate these cellular

396   processes and account for their mutual dependence. A similar dependence between cellular

397   contributions is observed in the pupal wing, where the constant tissue area is maintained by

398   epithelial tension via extracellular matrix connections to the cuticle (Etournay et al. 2015). We

399   do not yet know whether the larval wing disc is mechanically constrained. It will be interesting

400   to explore whether the extracellular matrix has anisotropic properties or whether the folding

401   pattern of the tissue influences growth orientation.

402   The fact that Fat PCP mutant wings are associated with less anisotropic clone shapes

403   and more weakly oriented cell divisions (Baena-López et al. 2005; Mao et al. 2011) has led to the

404   idea that Fat orients growth through its effect on cell division orientation. We find that shear

405   due to cell divisions cannot fully account for the anisotropy of growth, however. This result

406   suggests either that there are other orienting factors, or that Fat PCP has more profound effects

407   on growth anisotropy than can be accounted for by cell division.

408   Overall, this work open new avenues towards an understanding of wing morphogenesis

409   that integrates different scales – from the larval hormonal networks, to the morphogen-

410   dependent patterns of cell dynamics from which tissue shape emerges.

411

412   **Figure legends**

413   **Figure 1: 20E is sufficient to stimulate prolonged cell division in cultured wing discs**

414   Wing discs from mid-third instar larvae (96hr AEL) were cultured for indicated times

415   and then stained with phospho-Histone H3 to detect mitotic nuclei at the indicated timepoints.

416   (A) Representative images and (B) their quantification. Scale bar indicates 50μm. Discs were

417   given (i) no hormone supplement, (ii) 5μg/ml insulin, (iii) 20nM 20E or (iv) both. In (v) is an

418   image of an uncultured disc from the beginning of the experiment (96hr AEL). In (B), we show

419   pooled results from multiple experiments from different days. Each dot is the mean density of

420   mitotic nuclei (# nuclei per $10\times10\mu m^2$ area, averaged across the pouch from a single disc). Discs

421   from experiments performed on the same day have the same color. The box plots summarize all

422   data for each condition. Hinges correspond to the first and third quartiles; lines extend to the

423   highest and lowest values within 1.5*IQR (inter-quartile range); outlier points are black. n.d. =

424   not determined. (C) Apical cell area the wing pouch after 9hr of culture. Overall, the morphology

425   is maintained during culture, except in presence of both hormones. Lowering the concentration

426   of 20E in combination with insulin does not further prolong proliferation (See Fig. 1--Figure

427   Supplement 1).

428

429   **Figure 2: Size and overlap of the direct transcriptional responses to 20E or insulin**

430   Transcriptomes of wing discs cultured in either 20E or insulin were sequenced and

431   compared to those of uncultured discs and discs cultured without any hormone. A gene was

432   classified as hormone-dependent if its levels changed upon culture without hormone and

433   responded in the correct direction (more similar to uncultured levels) when cultured with

434   hormone. (A) Total number of genes that responded to 20E or insulin at two timepoints. (B)

435   Overlap between the hormone-dependent responses at 4hr (left), 9hr (right) or when each

436   hormone supports the most amount of proliferation (4hr for insulin, 9hr for 20E). Circles are all

437   drawn to scale. Numbers denote the amount of genes in the overlapping or non-overlapping

438   sets.

439

440   **Figure 3: Processes that are transcriptionally regulated by insulin in cultured discs**

441   Shown are the Biological Process (BP) Gene Ontology (GO) terms that are significantly

442   enriched in the set of genes identified to be activated (A) or repressed (B) by insulin in cultured

443   wing discs (simplified with a semantic similarity algorithm; threshold=0.95). In both (A) and

444   (B), we plot the GO terms according to the fraction of its total genes that were identified in the

16

445   data (# genes in the data with this GO term/total size of the GO term). The size of the point

446   indicates the significance of enrichment (BH-corrected p-value; cutoff of p <0.005). The color

447   indicates either 4hr (light orange in A, green in B) or 9hr of culture (dark orange in A, dark

448   green in B). Note that by 9hr of culture in insulin, no GO terms are enriched in the group of

449   genes repressed by insulin (B). Asterisks indicate terms shared by both insulin and 20E. Note

450   that many categories are only enriched (or more significantly enriched) at 4hr. This transience

451   in the response to insulin must result from downregulation of the pathway at a point

452   downstream of PI3K activation, since a fluorescent reporter of this enzyme's activity indicates

453   that it is still active for the duration of culture (See Fig. 3--Figure Supplement 2).

454

455   **Figure 4: Processes that are transcriptionally regulated by 20E in cultured discs**

456   Shown are the Biological Process (BP) Gene Ontology (GO) terms that are significantly

457   enriched in the set of genes identified to be activated (A) or repressed (B) by 20E in cultured

458   wing discs (simplified with a semantic similarity algorithm; threshold=0.9). In both (A) and (B),

459   we plot the GO terms according to the fraction of its total genes that were identified in the data

460   (# genes in the data with this GO term/total size of the GO term). The size of the point indicates

461   the significance of enrichment (BH-corrected p-value; cutoff of p <0.005). The color indicates

462   either 4hr (light orange in A, green in B) or 9hr of culture (dark orange in A, dark green in B).

463   Asterisks indicate terms shared by both insulin and 20E.

464

465   **Figure 5: Patterning and morphogenesis genes that are regulated by 20E in culture**

466   Normalized expression values are plotted across all conditions for selected 20E-

467   regulated genes. The expression value of each gene (fkpm) is shown relative to its expression in

468   uncultured discs, $\log_2(x/\text{uncultured})$. Genes were plotted on one of two scales (labeled as 1 or

469   2), depending on how much its values changed across conditions. Yellow squares indicate genes

470   with published loss-of-function phenotypes in the wing. Previously identified 20E-targets and

471   genes with known connections to specific patterning systems (in any context) are indicated.

472

473   **Figure 6: Widespread effects on morphogen signaling and PCP upon perturbation of 20E**

474   **signaling *in vivo***

475   A dominant-negative allele of EcR-B1 (W650A, abbreviated EcR-DN) was overexpressed

476   for 24hr in the dorsal compartment of the wing pouch using apterous-GAL4 and temperature-

477   sensitive GAL80. As a negative control performed in parallel, we overexpressed the wild type

478   EcR-B1 gene (EcR-WT), which does not significantly affect growth or proliferation of the disc

479   (Fig. 6--Figure Supplement 1) (A). Quantification of the expression patterns in this experiment

480   was done in one of two ways, each demonstrated in (A) for Discs-large (i), a septate junction

481   marker. The first scheme (Aii) was used for proteins in (B) and (D): the intensity profile

482   (arbitrary units) along a line in the Anterior compartment, drawn from Dorsal to Ventral, was

483   compared between EcR-WT and EcR-DN expressing discs. For Discs-large (Aii), this profile is

484   unaffected by EcR-DN expression. In contrast, intensity in the dorsal (pink shaded)

485   compartments is altered for the morphogen Wg (Bi), the Notch ligand Delta (Bii), adhesion

486   protein E-Cadherin (Biii), the HSPG Dallylike (Biv), the core PCP component Flamingo (Di) and

487   the Fat PCP component Dachsous (Dii). The lower images of parts Di-ii are zoomed-in regions

488   from the anterior compartment of the above images. The effect on the stripe of Wg expression

489   was confirmed by expressing EcR-DN in the posterior compartment (Fig. 6--Figure Supplement

490   2). The second scheme (Aiii) was used for the Hh/Dpp pathways (C): the profile of absolute

491   intensity along a line drawn from Anterior to Posterior in the Dorsal compartment (pink) was

492   compared to that along a line drawn in the Ventral compartment (black). For Discs-large (Aiii),

493   the black and pink lines are similar, both in EcR-WT (left) and EcR-DN (right) expressing discs.

494   However, a readout of Dpp signaling, pMAD (Ci) was affected, particularly in the posterior

495   compartment, by EcR-DN expression. In addition, compartment-autonomous differences in the

496   Hh pathway were observed: at the level of Hh itself (Cii), its transcriptional coactivator Ci (Ciii),

497   and the downstream target Engrailed (Civ). The effect of perturbing 20E signaling on Wg, Hh, Ci,

498   Engrailed, and Discs-large were confirmed by an independent method (removal of circulating

499   20E) in Fig. 6--Figure Supplement 3. Scale bars for the zoomed regions in (D)are 20um;

500   elsewhere they are 50um. In all quantified intensity profiles, the solid line represents the mean

501   of several discs from the same experiment (precise # depicted in each graph), and the shaded

502   ribbon is the standard deviation. All images are shown with dorsal up and anterior to the left.

503

504   Figure 7: Quantification of tissue growth and its cellular contributions

505   Three E-Cadherin-GFP-expressing wing discs were imaged for >13hr, and cells in the

506   future wing blade region were segmented and tracked. (A) Tissue shear was accumulated

507   between 2hr and 13hr in local regions of the tissue defined by a grid. Accumulated shear is

508   represented by blue bars plotted on outlines of the tracked region at 2hr (grey) and 13hr

509   (black). (B) The trace of the velocity gradient tensor $v = \partial_x v_x + \partial_y v_y$ quantifies the relative

510   change of tissue area. The diagonal component of the traceless symmetric part of the velocity

511   gradient tensor $\tilde{v}_{xx} = \frac{\partial_x v_x + \partial_y v_y}{2}$ quantifies the tissue shear flow along x- and y-axes. (i) Relative

512   change of tissue area, accumulated from the start of the timelapse, contains contributions from

513   average cell area change, cell divisions and cell extrusions. In all experiments, positive tissue

514   area growth (blue) is driven by cell divisions (orange) and partially opposed by cell extrusions

515   (cyan) and cell area change (green). (ii) Accumulated tissue shear along the x-axis, averaged

516   over the entire tracked region is plotted as a function of time (blue). The continuous shear of the

517   blade perpendicular to the x-axis (negative values of blue curve) is composed of similar

518   contributions from cell elongation change (green), T1 transitions (red) and cell divisions

519   (orange). Contributions from cell extrusions (cyan) and correlations (magenta) are negligible.

520   (iii-iv) Velocity gradient components $\partial_x v_x$, and $\partial_y v_y$ represent tissue extension or compression

521   along the x- and y-axis, respectively. We calculated the accumulated extensions along x- and y-

522   axes from the relative area change of the tissue and the tissue shear. Cellular contributions to

523   the tissue expansion along the x-axis were determined as described in the Methods. We find that

524   the tissue does not extend along the x axis (blue line in iii), although cell divisions do contribute

525   to tissue expansion along the x axis (orange line in iii). In contrast, tissue extension along the y

526   axis (blue line in iv) closely follows the cell division contribution (orange line in iv). The sum of

527   other contributions is small.

19

528   **MATERIALS AND METHODS**

529

530   **Flies**

531   The culture experiments described in Fig. 1 and the transcriptomic analyses were

532   performed using wild type OregonR *Drosophila*. For live imaging experiments, we used animals

533   in which the endogenous E-Cadherin gene had been fused with GFP (Huang et al. 2009). To

534   enable temperature inducible GAL4-dependent gene expression, we combined the *apterous-*

535   *GAL4* (Marois et al. 2006)*, phantom-GAL4* (Ono et al. 2006) and *engrailed-GAL4* (DeVido et al.

536   2008) loci with the temperature-sensitive GAL4 repressor GAL80[ts] driven by the tubulin

537   promoter. UAS-EcR.B1 (BDSC 6469) and UAS-EcR.B1-DeltaC655.W650A (BDSC 6872) were

538   acquired from Bloomington Stock Center (Bloomington, Indiana, USA). The line used to induce

539   RNAi against *neverland* was obtained from the group of R. Niwa (Yoshiyama et al. 2006).

540   Flies were grown on standard media containing cornmeal, molasses agar and yeast

541   extract under a 12hr light/dark cycle at 25°C (except when gene expression was induced using

542   the temperature-sensitive GAL80, described below).

543   For all disc culture experiments, we used wing discs from larvae at 96hr after egg laying

544   (AEL). Flies were allowed to lay eggs on apple juice agar plates (supplemented with yeast paste)

545   for 1-2hr at 25°C. Agar pieces containing ∼10-12 eggs each were placed into food vials and

546   grown at 25C°C. The middle of the egg collection window was considered to be 0hr AEL.

547

548   **Wing disc culture**

549   *Culture media:*

550   Early experiments (data not shown) indicated that overall disc morphology was best

551   preserved in Grace's Insect culture medium, compared to Schneider's or Shield's and Sang. Thus,

552   Grace's was used for all experiments. Grace's medium (Sigma G9771) was prepared without

553   Sodium bicarbonate but with the addition of 5mM BisTris. The pH was adjusted to 6.6-6.7 at

554   room temperature, and the prepared liquid media was stored at 4°C for no longer than one

555   month. On the day of the experiment, we added 5% Fetal Bovine Serum

556   (ThermoFisher/Invitrogen 10270098) and Penicillin-Streptomycin (Sigma P4333, 100x) to

557   impede microbial growth. Note that while other groups have included female fly extract in the

558   media (Zartman et al. 2013; Handke et al. 2014; Tsao et al. 2016), we found it to be less

559   reproducible than FBS (data not shown). Furthermore, recent evidence indicates that fly extract

560   is associated with non-physiological calcium waves in explanted wing discs (Balaji et al. 2017).

561   Stock solutions of either 20E or insulin were added just prior to the start of the

562   experiment. 20E (Sigma H5142) was added as a 1:1000 dilution from an ethanol stock solution

563   (stored at -20°C, prepared fresh weekly) to give a final concentration of 20nM in the media

20

564   (except when otherwise noted). Bovine insulin (Sigma I5500) was prepared as a 10mg/ml stock

565   solution in acidified water (stored at -20°C) and added at a final concentration of 5µg/ml. This

566   concentration of insulin is comparable to the levels used in previous studies aimed at

567   prolonging proliferation of discs in culture (Zartman et al. 2013; Handke et al. 2014). Given that

568   our data on the proliferation index in discs cultured in insulin alone (Fig 1Bii) quantitatively

569   agree with the results of these previous studies, the other differences between our culture

570   media and theirs do not seem to be as important as hormonal content.

571

572   *Culture procedure:*

573   To prepare larvae for dissection, we first floated them out of the food by adding 30%

574   sucrose. Larvae were transferred using a brush or wide-tip transfer pipet into glass dishes.

575   Excess food was removed by washing in sucrose, followed by distilled water. They were then

576   surface sterilized by immersion in 70% ethanol for 1-2 min. Finally, they were washed once

577   more with sterile water and then media. Except for the live imaging experiments, discs were

578   dissected in hormone-free media and then immediately transferred from the dissecting well

579   into media containing hormone. For each experiment, dissections were performed over a period

580   of no more than 45min, and the start time of the culture was considered to be the midpoint of

581   that dissection window. The number of discs analyzed per sample was limited by how many

582   could be manually dissected as carefully as possible during that time window.

583   Discs were cultured in glass wells (Electron Microscopy Sciences, Hatfield, PA; 70543-

584   30) in 500µl of growth media, with 10-20 discs per well, at 25°C in humidified chambers. Media

585   was exchanged approximately every 2hr, except during the long incubations of 16-24hr, when

586   there was a maximum incubation without media change of 8hr. At the end of culture, discs were

587   fixed by exchanging the media with 4% PFA (8% PFA stock solution in PBS diluted 2X into

588   Grace's media). Discs were incubated for 20min at room temperature and stained as described

589   below in the immunofluorescence section.

590   The data presented in Fig. 1 represent a compilation of results from multiple days

591   (labeled in different colors). Two replicates were done for each hormonal condition and

592   timepoint. All discs were included in the analysis, except in rare cases when a disc was distorted

593   during mounting.

594

595   **Transcriptomic analysis**

596   *Sample preparation*

597   Three biological replicates were performed for each hormone condition and timepoint.

598   For each, ~20-30 discs were dissected and cultured as described above and then transferred to

599   a microfuge tube in a volume of 15-20µl (growth media). Discs were frozen immediately in

21

600 liquid nitrogen and stored at -80℃ until all samples were ready for RNA isolation. A Qiagen

601 RNeasy Mini kit was used to isolate RNA for sequencing. Samples were lysed by adding Buffer

602 RLT + 2-mercaptoethanol and vortexing for 20-30 seconds on ice. The manufacturer's

603 instructions were followed for the rest of the protocol. Further purification was achieved with

604 an ethanol precipitation.

605

606 *Sequencing*

607   mRNA was isolated from 1μg total RNA by poly-dT enrichment using the NEBNext

608 Poly(A) mRNA Magnetic Isolation Module according to the manufacturer's instructions (New

609 England Biolabs). Final elution was done in 15μl of 2x first strand cDNA synthesis buffer. After

610 chemical fragmentation by incubating for 15 min at 94°C, the sample was directly subjected to

611 the workflow for strand-specific RNA-Seq library preparation (Ultra Directional RNA Library

612 Prep, New England Biolabs). For ligation, custom adaptors were used (Adaptor-Oligo 1: 5'-ACA-

613 CTC-TTT-CCC-TAC-ACG-ACG-CTC-TTC-CGA-TCT-3', Adaptor-Oligo 2: 5'-P-GAT-CGG-AAG-AGC-

614 ACA-CGT-CTG-AAC-TCC-AGT-CAC-3'). After ligation, adapters were depleted with an XP bead

615 purification (Beckman Coulter), adding beads in a ratio of 1:1. Indexing was done during the

616 following PCR enrichment (15 cycles) using custom amplification primers carrying the index

617 sequence indicated with 'NNNNNN'. (Primer1: Oligo_Seq 5'-

618 AATGATACGGCGACCACCGAGATCTACACTCTTTCCCTACACGACGCTCTTCCGATCT-3', primer2: 5'-

619 GTGACTGGAGTTCAGACGTGTGCTCTTCCGATCT-3', primer3: 5'-

620 CAAGCAGAAGACGGCATACGAGAT NNNNNN GTGACTGGAGTT-3'. After two more XP beads

621 purifications (1:1), libraries were quantified using Qubit dsDNA HS Assay Kit (Invitrogen).

622 Equimolar amounts of each sample were pooled and distributed amongst four lanes of an

623 Illumina HiSeq 2500 sequencer for 75bp single-end sequencing. On average we achieved 37

624 million reads per sample.

625

626 *Processing of sequencing data*

627   Short read data was trimmed using Cutadapt (Martin 2011) and aligned using TopHat2

628 (Kim et al. 2013). Differential gene expression analysis was performed for all pairwise

629 comparisons between conditions and timepoints using Cufflinks (Trapnell et al. 2012). Our

630 threshold for significance was q<0.01. We considered a gene to be expressed if it had a

631 normalized count of fpkm (fragments per kilobase of transcript per million mapped reads) > 5.

632   Raw sequencing data and fpkm normalized expression data files have been deposited in

633 NCBI's Gene Expression Omnibus and are accessible through GEO Series accession number

634 GSE92933.

635

636 *Analysis of hormone-responsive genesets*

637 The identification of hormone-responsive genesets was achieved by selectively filtering

638 the differentially expressed genes table from Cufflinks using custom R scripts. First, we

639 identified the genes in this table whose levels were significantly different (q<0.01) between no

640 culture (freshly dissected discs) and culture without hormone. We split this culture-responsive

641 subset into two groups based on whether their levels in uncultured discs were abnormally low

642 or high after culture without hormone. To identify hormone-activated genes, we first identified

643 the genes whose expression was abnormally low in culture with no hormone (relative to

644 uncultured control). Amongst these, we identified genes whose levels were significantly

645 elevated (either at 4hr or 9hr) when discs were culture with hormone (compared to culture

646 with no hormone). Hormone-repressed genes had the opposite pattern: abnormally high when

647 cultured without hormone but significantly lower in culture with hormone.

648 The Venn diagrams presented in Fig. 2 were generated using the VennDiagram package

649 of R (Chen & Boutros 2011) after identifying the genes that were unique or common in each

650 pairwise comparison.

651 We identified enriched Gene Ontology (GO) terms (Biological Process and Cellular

652 Component) within each hormone-responsive dataset using the R-package ClusterProfiler (v

653 1.9) (Yu et al. 2012). To reduce redundancy, we used the simplify function of this package;

654 similarity and p-value cutoffs are written in the figure legends. We also required enriched GO

655 terms to have > 5 genes included in the data.

656 For selected genes, we plotted the expression levels across all conditions (Fig. 3-Figure

657 Supplement 1, Fig. 4-Figure Supplement 1, Fig. 5) by taking the $\log_2$ of the normalized counts

658 (fkpm) in each condition divided by that in the uncultured wing discs.

659 For the 589 genes regulated by 20E (either exclusively or also by insulin), we manually

660 classified functional groupings after reviewing related literature, GO term assignments, and

661 Flybase annotations. The classifications used in Fig. 4-Figure Supplement 1 and Fig. 5 are

662 explained as follows: DNA replication/cell cycle includes anything having a positive effect on

663 DNA replication and/or cell cycle progression. Cell death/DNA damage includes genes

664 annotated with a function in apoptosis, programmed cell death, or DNA repair. Protein

665 production includes splicing, translation, ribosome biogenesis, and protein folding. Nutrient

666 transport was limited to proven or predicted members of the SLC/MFS superfamily. The

667 patterning group includes anything known to regulate or be a target of developmental signaling

668 pathways (in any system, not limited to the wing disc). The transcription/chromatin class

669 included verified and putative transcription factors and chromatin modifying proteins. Tissue

670 morphogenesis includes genes involved in cell-cell or cell-ECM contact, as well as cytoskeletal

671 components and regulators. Lastly, the sugar modifications group describes anything involved

23

672 in protein glycosylation. In Fig. 4-Figure Supplement 1, TOR targets were identified in (Teleman

673 et al. 2008; Guertin et al. 2006), and FOXO targets were from (Teleman et al. 2008; Puig et al.

674 2003; Spellberg et al. 2015; Alic et al. 2014). In Fig. 5, 20E targets are based on (Beckstead et al.

675 2005; Gauhar et al. 2009).

676   After examining these expression profiles, we realized that there were 11 genes that

677 appeared to change over time irrespective of hormone content and were thus falsely identified

678 as being 20E-responsive. We removed these genes from consideration in the heatmaps by

679 identifying those that responded equally well to both insulin and 20E at 9hr but to neither at

680 4hr.

681

Temperature-sensitive GAL4/GAL80^{ts} experiments

683   *Apterous-GAL4, GAL80^{ts}/CyO-GFP* females were crossed with males of *UAS-EcR* or *UAS-*

684 *EcR-W650A*, and their progeny were kept at 18°C (permissive for GAL80 repressor function) on

685 bromophenol blue-containing food for 7-8 days. Vials were then moved to 29°C (restrictive) to

686 induce GAL4-dependent transcript of EcR constructs for 24hr. Upcrawling larvae were selected

687 for dissection based on the absence of GFP and the presence of blue food in the gut (indicating

688 that they are still many hours from pupariation) (Andres & Thummel 1994).

689   To remove circulating 20E, *UAS-CD8-GFP;;phantom-GAL4, GAL80^{ts}/TM3-GFP* females

690 were crossed with males of the *neverland* targeting line, and their progeny were kept at 18°C.

691 Vials were shifted to 29°C, and discs from upcrawling larvae lacking the *TM3-GFP* balancer were

692 dissected 2 or 4 days later. As controls, we used progeny of *UAS-CD8-GFP;;phantom-GAL4,*

693 *GAL80^{ts}/TM3-GFP* females crossed to *w^{1118}* flies in parallel. The progeny of the control cross all

694 pupariated by 2 days after shift to 29°C.

695

Immunofluorescence

697   Primary antibodies used were: anti-Ci-full length (1:100, rat, DSHB 2A1 conc), anti-

698 Dally-like (1:100, mouse, DSHB 13G8 conc), anti-Dachsous (1:1000, mouse, (Merkel et al.

699 2014)), anti-Delta (1:800, mouse, DSHB C594.9B, conc), anti-Engrailed (1:100, mouse, DSHB

700 4D9 conc), anti-Discs-large (1:100, mouse, DSHB 4F3), anti-E-Cadherin (1:100, rat, DSHB

701 DCAD2 sup), anti-Flamingo (1:200, rabbit, (Sagner et al. 2012)), anti-Hh (1:500, rabbit, (Eugster

702 et al. 2007)), anti-Patched (1:100, mouse, DSHB Apa1 conc), anti-pHistoneH3-Ser10 (1:1000,

703 rabbit, Cell Signaling, Danvers, MA, USA), anti-pMAD (1:1000, rabbit, Epitomics, Burlingame, CA,

704 USA), anti-Wg (1:100, mouse, DSHB 4D4). DSHB stands for Developmental Studies Hybridoma

705 Bank (Iowa, USA).

706   Secondary antibodies used were: Alexa-fluor-488 goat anti-Rabbit (1:1000,

707   ThermoFisher A11034), Alexa-fluor-555 goat anti-Mouse (1:1000, ThermoFisher A21424),

708   Alexa-fluor-647 goat anti-Rat (1:500, ThermoFisher A21247)

709   Discs were dissected in PBS and then fixed for 20min at room temperature in 4%

710   PFA/PBS. Samples were permeabilized by rinsing twice with PBS+0.1% TritonX100 (TPBS) and

711   blocked with TPBS +0.1mg/ml BSA + 250mM NaCl for 45-60min at room temperature. They

712   were then incubated overnight at 4°C in primary antibody solution made in PBS+0.1%

713   TritonX100+0.1mg/ml BSA (BBX). The next day, stainings were washed in BBX, followed by

714   BBX+4% normal goat serum. Samples were then incubated at room temperature for 2-4hr in

715   the dark with secondary antibodies diluted in BBX. Finally, samples were washed several times

716   in TPBS and mounted between a glass slide and coverglass separated by a double-sided tape

717   spacer. The discs were oriented with their apical surface toward the coverglass and immersed

718   in VectaShield mounting medium (Vector Laboratories H-1000).

719   Imaging of fixed samples was performed using an Olympus FV1000 laser scanning

720   confocal microscope fitted with an Olympus BX61 inverted stand and motorized XYZ stage,

721   driven by FV10-ASW 1.7 software. Wing discs were imaged using either an Olympus

722   UApochromat 40X 1.35NA oil immersion or Olympus UPlanSApochromat 60X 1.35NA oil

723   immersion objective.

724   All discs were imaged and analyzed, except in very rare cases when the discs were

725   damaged or misshapen during mounting.

726

727   **Analysis of immunofluorescence images**

728   *Phospho-Histone H3*

729   Z-stacks of wing discs stained with PH3, E-Cadherin, Patched and Wingless were

730   analyzed in 2D after a maximum intensity projection. PH3+ nuclei were segmented using FIJI

731   Weka segmentation plugin (Arganda-Carreras et al. 2017). A training set containing images

732   from each condition of the experiment was used to generate a common classifier, which was

733   then applied to all images. Probability masks were thresholded by likelihood and size. We

734   quantified signal only in the wing pouch, which was identified morphologically by the innermost

735   folds in the epithelium. Compartment and wing pouch size in Fig. 6-Figure Supplement 1 was

736   measured on a 2D projection, using FIJI to manually identify the region of interest. Plotting was

737   performed in R.

738

739   *Cell area in fixed samples*

740   In Fig. 1C, apical cell areas were determined and plotted using Tissue Analyzer (Aigouy

741   et al. 2016) to segment cells based on E-Cadherin staining, and Tissue Miner (Etournay et al.

742   2016) to determine the area and position of each cell.

743

744   *Intensity profiles*

745   The changes to patterns of protein production/localization upon *in vivo* perturbation of

746   20E signaling were analyzed in a 2D maximum intensity projection. Using Fiji (Schindelin et al.

747   2012), a line 50 pixels wide (~20μm) was drawn either from dorsal to ventral in the anterior

748   and posterior compartments or from anterior to posterior in the dorsal and ventral

749   compartments. Absolute intensity values along these lines were averaged across all samples

750   (imaged on the same day, under the same acquisition settings). Plotted is the mean and

751   standard deviation of intensity along these lines. At least five discs were imaged per biological

752   condition; exact numbers are shown in the figures.

753

754   **Long-term timelapse imaging**

755   Discs were dissected directly in growth media containing hormone. For imaging, discs

756   were gently immobilized under a porous filter (Whatman cyclopore polycarbonate membranes,

757   Sigma WHA70602513) in a 35mm glass-bottomed Petri dish (Mattek, Ashland, MA, USA; P35G-

758   1.0-14-C) using double stick tape (Tesa 5338, doppelband fotostrip, ~100μm thick) as a spacer

759   between the glass and the filter. To construct this chamber, we first punched a hole (6mm) in

760   the tape, and then adhered the tape to the glass. The discs were transferred in ~10μl media to

761   the center of the hole in the tape spacer. Care was taken to keep the tape dry. Discs were

762   carefully arranged to be apical-side down (toward coverslip) using forceps. Most of the media

763   was then removed, and the filter (cut approximately to the size of the tape) was quickly placed

764   over the sample and firmly adhered to the tape with forceps. The dish was then filled with 2-3ml

765   media. The height of these chambers is somewhat greater than the height of the discs, but the

766   presence of the filter isolates the discs from flows and somewhat constrains disc movements so

767   that they usually remain in the field of view. As an alternative, we also tried to immobilize discs

768   using methylcellulose (Aldaz et al. 2010) dissolved in our culture medium, but discs do not

769   proliferate in this condition.

770   During imaging, we used a syringe pump (PHD ULTRA, Harvard Apparatus, Cambridge,

771   MA, USA) to automatically and continuously exchange the media during the course of imaging at

772   a rate of 0.03 ml/min. The start of the movie was considered to be time 0hr. This time

773   corresponds to 45-60min from the start of dissection (time required for sample preparation and

774   microscope setup).

775   Imaging was performed using a Zeiss spinning disc microscope consisting of an

776   AxioObserver inverted stand, motorized xyz stage with temperature control set to 25℃,

777   Yokogawa CSU-X1 scanhead, and a Zeiss AxioCam MRm camera (2x2 binning), all controlled by

778   Axiovision software. Discs were imaged through a Zeiss C-Apochromat 63X 1.2NA water

779   immersion objective heated to 25℃ with an objective heater. To capture the whole pouch, we

780   acquired a 2x2 tiled region (10% overlap). Each region consisted of a Z-stack of 65-85 frames,

781   spaced 0.5μm apart. Tiled Z-stacks were captured every 5min. We kept light exposure as low as

782   possible to achieve a segmentable image. We used a power meter (PT9610, Gigahertz-optik,

783   Munich, Germany) to measure the power of the laser through a 10x/0.45 NA objective within a

784   week of the experiment. For imaging, we used a laser power of 0.04-0.05 mWatts and an

785   exposure time of 350ms per image.

786

787   **Analysis of live imaging**

788   *Image processing, segmentation, and cell tracking*

789   Raw data was first processed with a low-pass frequency filter to remove high frequency

790   noise, followed by a rolling ball background subtraction algorithm using FIJI (Schindelin et al.

791   2012). The apical plane was projected onto 2D using a custom-made algorithm. We identified

792   the two manifolds formed by the disc proper layer and the peripodial layer, respectively, in the

793   3D z-stacks, based on maximal brightness of the E-Cadherin-GFP signal and subject to hard

794   constraints on the distance between the two layers and the slope of each manifold. We

795   employed the algorithm of Wu and Chen (Wu & Chen 2002) to simultaneously determine the

796   two manifolds that are optimal, i.e. as bright as possible under the given constraints. This

797   algorithm and its application to the wing disc will be described in detail in a separate upcoming

798   manuscript.

799   Projected tiles were stitched using the Grid/Collection Stitching FIJI plugin (Preibisch et

800   al. 2009). Segmentation and cell tracking was performed on the projected images of the

801   timelapse using Tissue Analyzer (Aigouy et al. 2016).

802   Cells within the wing pouch of the disc, as well as those on either side of the AP and DV

803   boundaries, were manually marked using Tissue Miner (Etournay et al. 2016). The AP boundary

804   is detectable on the basis of larger apical areas of the cells on either side, straighter cell

805   boundaries at the interface and a slight reduction of E-Cadherin intensity on its anterior side.

806   The DV boundary is detectable on the basis of increased E-Cadherin intensity and reduced

807   apical areas of cells on either side of the boundary. All analysis was performed on the subset of

808   cells within the pouch that were trackable throughout the entire course of the movie, excluding

809   cells that move in or out of the field of view.

810

Analysis of cellular contributions to changes in tissue size and shape

811
812 The accumulated local tissue shear presented in Fig. 7A was obtained by dividing the
813 tissue using a rectangular grid and calculating the tissue shear in each grid element as described
814 previously (Etournay et al. 2016; Etournay et al. 2015). The blue bars represent the cumulative
815 sum of tissue shear in each region, starting from 2hr (after the adaptation phase) and
816 continuing to the end of the movie. For this calculation, we considered only grid elements with
817 triangles covering more than half of the grid element area.
818 We quantify the relative area change rate and shear rate, averaged in the tracked wing
819 pouch region, and the corresponding cellular contributions using the Triangle Method (Merkel
820 et al. 2017). The relative area change decomposition states

821
$$v = \frac{1}{a}\frac{da}{dt} + k_d - k_e,$$

822 where a is the average cell area and k_d and k_e are cell division and extrusion rates. The relative
823 area change rate v corresponds to the trace of the velocity gradient tensor $\partial_i v_j$. The indices i
824 and j take values x and y. In Fig. 7Bi, we plot the accumulated relative area change of the
825 tracked region of the wing pouch $\int_0^t v\, dt$ (blue line), accumulated relative change of the average
826 cell area $\int_0^t \frac{1}{a}\frac{da}{dt} dt$ (green line), accumulated contribution due to cell divisions $\int_0^t k_d\, dt$ (orange
827 line) and the accumulated contribution due to cell extrusions $\int_0^t k_e\, dt$ (cyan line).

828 The decomposition of the shear rate into its cellular contributions is

829
$$\tilde{v}_{ij} = \frac{DQ_{ij}}{Dt} + T_{ij} + C_{ij} + E_{ij} + D_{ij},$$

830 where Q_{ij} is the cell elongation tensor and D/Dt is a corotational derivative (Merkel et al.
831 2017). T_{ij}, C_{ij}, E_{ij} and D_{ij} are contributions to the shear rate from T1 transitions, cell divisions,
832 cell extrusions and correlation effects, respectively. In Fig. 7Bii we plot the accumulated xx
833 component of shear of the tracked region $\int_{t_0}^t \tilde{v}_{xx}\, dt$ (blue line), accumulated xx component of
834 shear due to cell elongation change $\int_{t_0}^t \frac{DQ_{xx}}{Dt} dt$ (green line), accumulated xx component of shear
835 due to T1 transitions $\int_{t_0}^t T_{xx}\, dt$ (red line), accumulated xx component of shear due to cell
836 divisions $\int_{t_0}^t C_{xx}\, dt$ (orange line), accumulated xx component of shear due to cell extrusions
837 $\int_{t_0}^t E_{xx}\, dt$ (cyan line) and accumulated xx component of shear due to correlation effects
838 $\int_{t_0}^t D_{xx}\, dt$ (magenta line). The x-axis of the coordinate system is parallel to the DV boundary as
839 explained in the main text. The initial timepoint is $t_0 = 2$hr.

840   The expansion of the wing pouch along the x-axis and the expansion along y-axis

841   perpendicular to it are quantitatively described by velocity gradient components $\partial_x v_x$ and $\partial_y v_y$,

842   respectively. These components of the velocity gradient tensor are determined from v and $\tilde{v}_{xx}$

843   as

844
$$\partial_x v_x = \frac{1}{2} v + \tilde{v}_{xx}$$

845
$$\partial_y v_y = \frac{1}{2} v - \tilde{v}_{xx} \,.$$

846   We then decompose the velocity gradient components into cellular contributions using the

847   decompositions of v and $\tilde{v}_{xx}$ as follows

848
$$\partial_x v_x = \left(\frac{1}{2}\frac{1}{a}\frac{da}{dt} + \frac{DQ_{xx}}{Dt}\right) + T_{xx} + \left(\frac{1}{2}k_d + C_{xx}\right) + \left(\frac{1}{2}k_e + E_{xx}\right) + D_{xx}\,,$$

849
$$\partial_y v_y = \left(\frac{1}{2}\frac{1}{a}\frac{da}{dt} - \frac{DQ_{xx}}{Dt}\right) - T_{xx} + \left(\frac{1}{2}k_d - C_{xx}\right) + \left(\frac{1}{2}k_e - E_{xx}\right) - D_{xx}\,.$$

850

851   Here, $\frac{1}{2}\frac{1}{a}\frac{da}{dt} \pm \frac{DQ_{xx}}{Dt}, \pm T_{xx}, \frac{1}{2}k_d \pm C_{xx}, \frac{1}{2}k_e \pm E_{xx}$ and $\pm D_{xx}$ are the contributions to the velocity

852   gradient component from cell shape change, T1 transitions, cell divisions, cell extrusions and

853   correlations, respectively. The upper sign is used in the decomposition of $\partial_x v_x$ and lower sign in

854   the decomposition of $\partial_y v_y$.

855   In Fig. 7Biii we plot the accumulated wing pouch expansion along the x-axis $\int_{t_0}^{t} \partial_x v_x \, dt$

856   (blue line), accumulated cell shape expansion along the x-axis $\int_{t_0}^{t} \left(\frac{1}{2}\frac{1}{a}\frac{da}{dt} + \frac{DQ_{xx}}{Dt}\right) dt$ (green line),

857   accumulated contribution to the expansion along the x-axis due to T1 transitions $\int_{t_0}^{t} T_{xx} \, dt$ (red

858   line), accumulated contribution to the expansion along the x-axis due to cell divisions

859   $\int_{t_0}^{t} \left(\frac{1}{2}k_d + C_{xx}\right) dt$ (orange line), accumulated contribution to the expansion along the x-axis due

860   to cell extrusions $\int_{t_0}^{t} \left(\frac{1}{2}k_e + E_{xx}\right) dt$ (cyan line) and accumulated contribution to the expansion

861   along the x-axis due to correlation effects $\int_{t_0}^{t} D_{xx} \, dt$ (magenta line).

862   In Fig. 7Biv, we plot the accumulated wing pouch expansion along the y-axis $\int_{t_0}^{t} \partial_y v_y \, dt$

863   (blue line), accumulated cell shape expansion along the y-axis $\int_{t_0}^{t} \left(\frac{1}{2}\frac{1}{a}\frac{da}{dt} - \frac{DQ_{xx}}{Dt}\right) dt$ (green line),

864   accumulated contribution to the expansion along the y-axis due to T1 transitions $\int_{t_0}^{t} -T_{xx} dt$ (red

865   line), accumulated contribution to the expansion along the y-axis due to cell divisions

866   $\int_{t_0}^{t} \left(\frac{1}{2}k_d - C_{xx}\right) dt$ (orange line), accumulated contribution to the expansion along the y-axis due

867   to cell extrusions $\int_{t_0}^{t} \left(\frac{1}{2}k_e - E_{xx}\right) dt$ (cyan line) and accumulated contribution to the expansion

868   along the y-axis due to correlation effects $\int_{t_0}^{t} -D_{xx}\, dt$ (magenta line).

869   In both Fig. 7Biii and Fig. 7Biv the initial timepoint is $t_0 = 2$hr.

870

871   *Estimation of tracking errors*

872   Even if the cells are perfectly segmented in each frame of the timelapse, the automated

873   cell tracking can still produce errors in tracking. These errors include false positive and false

874   negative divisions, false positive extrusions and false positive cell appearances. The tracking

875   errors either falsely remove or add a cell to the tissue. Since the overall cell number does not

876   depend on the precision of tracking, the tracking errors always appear in pairs. For example, if a

877   cell track is lost from frame 1 to 2, it is given a new cell ID in frame 2. This one error would

878   cause the counting of a false extrusion (as the cell is thought to be lost in frame 1) and a false

879   cell appearance (to account for the arrival of a new unique track in frame 2). Alternatively, the

880   new cell ID in frame 2 could be attributed to a false cell division, if it is interpreted to be the

881   daughter of a (false) division by a neighboring cell. These pairs of false cell events occur close to

882   each other in space and time. We use this property to identify the tracking errors and adjust our

883   quantification of the cellular contributions to tissue area change accordingly.

884   We have never observed any insertion of new cells into the wing disc epithelium and we

885   thus assume that any cell appearance, not associated with a cell division, is due to an error in

886   either segmentation or tracking. We devised a method to independently identify candidates for

887   false positive and false negative divisions using the fact that just before the division, the apical

888   area of the cell increases significantly as the nucleus moves apically. We measure the maximal

889   cell area and the ratio of maximal cell area to the average of the cell area throughout the

890   timelapse for each cell. We then discriminate dividing and non-dividing cells by performing a k-

891   means classification on these two variables (Jones et al. 2001). One type of error that could not

892   be identified by this method might occur if the original tracking identifies two cell divisions for

893   the same cell where only one actually occurs. In these situations, when the divisions are

894   separated by less than six frames, we take the later division to be true and the earlier one to be

895   false. Using these candidates for dividing and non-dividing cells we construct a list of candidates

896   for false positive and false negative divisions in the original tracking.

897   Finally, we pair cell appearances with cell extrusions and false negative cell division

898   candidates, and then we pair the false positive cell division candidates with the remaining cell

899   extrusions and remaining false negative cell division candidates. The cell events we manage to

900   pair in this way we treat as false, and we adjust the cell event counting accordingly.

901   To construct pairs of these cell events where each event can appear at most once, we

902   introduce a distance measure between cell events A and B in time and space:

903
$$d(A, B) = \sqrt{\frac{1}{2}(f_A - f_B)^2 + (x_A - x_B)^2 + (y_A - y_B)^2}$$

904   where $x_{A,B}$ and $y_{A,B}$ are coordinates of the cell centers (in pixels) in frame $f_{A,B}$ of the cell event,

905   for each of the two cell events. We then iteratively construct pairs of false cell events from all

906   possible combinations by repeating the following steps:

907   find a cell event pair with minimum d(A,B)

908   o   if d(A, B) > 25 stop the procedure

909   o   if d(A, B) < 25 identify pair (A, B) as a pair of false cell events

910   o   remove the events A and B from consideration in future iterations

911   This method identifies more than 90% of the cell appearances as false. It also finds that

912   between 85-90% of cell divisions and 45-75% of cell extrusions initially identified by Tissue

913   Analyzer were true events and that between 10-20% of true divisions were not recognized by

914   Tissue Analyzer. We used the corrected numbers of cell divisions and extrusions to calculate

915   contributions to tissue area change. The remaining number of cell appearances is very low

916   (<10) in all three experiments and not shown in the relative area change plots. This method

917   does not identify the daughter cells. Therefore, in the shear calculation by the Triangle Method,

918   we used the original tracking by the Tissue Analyzer. If we assume that the errors in cell

919   division tracking are not correlated with the cell division orientation and that the falsely

920   identified cell divisions are not oriented on average, we can estimate the relative error of the

921   shear due to cell divisions to be equal to the fraction of true division events not recognized by

922   the Tissue Analyzer i.e. 10-20%.

923

931

932   **COMPETING INTERESTS:**

933   The authors declare that they have no competing interests.

934

935

REFERENCES:

Aegerter-Wilmsen, T. et al., 2012. Integrating force-sensing and signaling pathways in a model for the regulation of wing imaginal disc size. *Development (Cambridge, England)*, 139(17), pp.3221–31.

Affolter, M. & Basler, K., 2007. The Decapentaplegic morphogen gradient: from pattern formation to growth regulation. *Nature reviews. Genetics*, 8(9), pp.663–674.

Aigouy, B., Umetsu, D. & Eaton, S., 2016. Segmentation and Quantitative Analysis of Epithelial Tissues. In pp. 227–239.

Aldaz, S., Escudero, L.M. & Freeman, M., 2010. Live imaging of Drosophila imaginal disc development. *Proceedings of the National Academy of Sciences of the United States of America*, 107(32), pp.14217–22.

Alic, N. et al., 2014. Interplay of dFOXO and Two ETS-Family Transcription Factors Determines Lifespan in Drosophila melanogaster S. K. Kim, ed. *PLoS Genetics*, 10(9), p.e1004619.

Ambegaonkar, A.A. et al., 2012. Propagation of dachsous-fat planar cell polarity. *Current Biology*, 22(14), pp.1302–1308.

Andres, A.J. & Thummel, C.S., 1994. Methods for quantitative analysis of transcription in larvae and prepupae. *Methods in cell biology*, 44, pp.565–73.

Arganda-Carreras, I. et al., 2017. Trainable Weka Segmentation: a machine learning tool for microscopy pixel classification. *Bioinformatics*, 9, pp.676–682.

Arquier, N. et al., 2008. Drosophila ALS Regulates Growth and Metabolism through Functional Interaction with Insulin-Like Peptides. *Cell Metabolism*, 7(4), pp.333–338.

Aw, W.Y. & Devenport, D., 2016. Planar cell polarity: Global inputs establishing cellular asymmetry. *Current Opinion in Cell Biology*.

Ayers, K.L. et al., 2012. Dally and Notum regulate the switch between low and high level Hedgehog pathway signalling. *Development*, 139(17), pp.3168–3179.

Ayers, K.L. et al., 2010. The Long-Range Activity of Hedgehog Is Regulated in the Apical Extracellular Space by the Glypican Dally and the Hydrolase Notum. *Developmental Cell*, 18(4), pp.605–620.

Baena-López, L.A., Baonza, A. & García-Bellido, A., 2005. The orientation of cell divisions determines the shape of Drosophila organs. *Current biology : CB*, 15(18), pp.1640–4.

Balaji, R. et al., 2017. Calcium spikes, waves and oscillations in a large, patterned epithelial tissue. *Scientific Reports*, 7, p.42786.

Beckstead, R.B., Lam, G. & Thummel, C.S., 2005. The genomic response to 20-hydroxyecdysone at the onset of Drosophila metamorphosis. *Genome Biology*, 6(12), p.R99.

Beira, J. V. & Paro, R., 2016. The legacy of Drosophila imaginal discs. *Chromosoma*, 125(4), pp.573–592.

Bodenstein, D., 1943. Hormones and tissue competence in the development of Drosophila. *The Biological Bulletin*, 84(1), pp.34–58.

Bornemann, D.J. et al., 2004. Abrogation of heparan sulfate synthesis in Drosophila disrupts the Wingless, Hedgehog and Decapentaplegic signaling pathways. *Development (Cambridge, England)*, 131(9), pp.1927–38.

Brennan, C.A. et al., 2001. Broad-complex, but not ecdysone receptor, is required for progression of the morphogenetic furrow in the Drosophila eye. *Development (Cambridge, England)*, 128(1), pp.1–11.

Brennan, C.A. et al., 1998. Ecdysone pathway is required for furrow progression in the developing Drosophila eye. *Development (Cambridge, England)*, 125(14), pp.2653–64.

Brittle, A., Thomas, C. & Strutt, D., 2012. Planar polarity specification through asymmetric subcellular localization of fat and dachsous. *Current Biology*, 22(10), pp.907–914.

Britton, J.S. & Edgar, B.A., 1998. Environmental control of the cell cycle in Drosophila: nutrition activates mitotic and endoreplicative cells by distinct mechanisms. *Development*, 125(11).

Bryant, P.J. et al., 1988. Mutations at the fat locus interfere with cell proliferation control and epithelial morphogenesis in Drosophila. *Developmental Biology*, 129(2), pp.541–554.

Bryant, P.J. & Levinson, P., 1985. Intrinsic growth control in the imaginal primordia of Drosophila, and the autonomous action of a lethal mutation causing overgrowth. *Developmental Biology*, 107(2), pp.355–363.

de Celis, J.F. & Bray, S., 1997. Feed-back mechanisms affecting Notch activation at the dorsoventral boundary in the Drosophila wing. *Development (Cambridge, England)*, 124(17), pp.3241–3251.

33

Chen, H. & Boutros, P.C., 2011. VennDiagram: a package for the generation of highly-customizable Venn and Euler diagrams in R. *BMC bioinformatics*, 12(1), p.35.

Cheng, L.Y. et al., 2011. Anaplastic lymphoma kinase spares organ growth during nutrient restriction in drosophila. *Cell*, 146(3), pp.435–447.

Clark, H.F. et al., 1995. Dachsous encodes a member of the cadherin superfamily that controls imaginai disc morphogenesis in Drosophila. *Genes and Development*, 9(12), pp.1530–1542.

Delanoue, R., Slaidina, M. & Léopold, P., 2010. The Steroid Hormone Ecdysone Controls Systemic Growth by Repressing dMyc Function in Drosophila Fat Cells. *Developmental Cell*, 18(6), pp.1012–1021.

DeVido, S.K. et al., 2008. The role of Polycomb-group response elements in regulation of engrailed transcription in Drosophila. *Development (Cambridge, England)*, 135(4), pp.669–676.

Etournay, R. et al., 2015. Interplay of cell dynamics and epithelial tension during morphogenesis of the Drosophila pupal wing. *eLife*, 4, p.e07090.

Etournay, R. et al., 2016. TissueMiner: A multiscale analysis toolkit to quantify how cellular processes create tissue dynamics. *eLife*, 5.

Eugster, C. et al., 2007. Lipoprotein-Heparan Sulfate Interactions in the Hh Pathway. *Developmental Cell*, 13(1), pp.57–71.

Fristrom, J.W., Logan, W.R. & Murphy, C., 1973. The synthetic and minimal culture requirements for evagination of imaginal discs of Drosophila melanogaster in vitro. *Developmental Biology*, 33(2), pp.441–456.

Garcia-Bellido, A. & Merriam, J.R., 1971. Parameters of the wing imaginal disc development ofDrosophila melanogaster. *Developmental Biology*, 24(1), pp.61–87.

Gauhar, Z. et al., 2009. Genomic mapping of binding regions for the Ecdysone receptor protein complex. *Genome research*, 19(6), pp.1006–13.

Géminard, C., Rulifson, E.J. & Léopold, P., 2009. Remote Control of Insulin Secretion by Fat Cells in Drosophila. *Cell Metabolism*, 10(3), pp.199–207.

Gershman, B. et al., 2007. High-resolution dynamics of the transcriptional response to nutrition in Drosophila: a key role for dFOXO. *Physiological genomics*, 29(1), pp.24–34.

Gibson, M.C. et al., 2006. The emergence of geometric order in proliferating metazoan epithelia. *Nature*, 442(7106), pp.1038–1041.

González-Gaitán, M., Capdevila, M.P. & García-Bellido, A., 1994. Cell proliferation patterns in the wing imaginal disc of Drosophila. *Mechanisms of Development*, 46(3), pp.183–200.

Guertin, D.A. et al., 2006. Functional Genomics Identifies TOR-Regulated Genes that Control Growth and Division. *Current Biology*, 16(10), pp.958–970.

Guirao, B. et al., 2015. Unified quantitative characterization of epithelial tissue development. *eLife*, 4(DECEMBER2015).

Hacker, U., Lin, X. & Perrimon, N., 1997. The Drosophila sugarless gene modulates Wingless signaling and encodes an enzyme involved in polysaccharide biosynthesis. *Development*, 124(18), pp.3565–3573.

Handke, B. et al., 2014. Towards long term cultivation of Drosophila wing imaginal discs in vitro. *PloS one*, 9(9), p.e107333.

Hartl, T.A. & Scott, M.P., 2014. Wing tips: The wing disc as a platform for studying Hedgehog signaling. *Methods*, 68(1), pp.199–206.

Heemskerk, I., Lecuit, T. & LeGoff, L., 2014. Dynamic clonal analysis based on chronic in vivo imaging allows multiscale quantification of growth in the Drosophila wing disc. *Development*, 141(11).

Heller, D. et al., 2016. EpiTools: An Open-Source Image Analysis Toolkit for Quantifying Epithelial Growth Dynamics. *Developmental Cell*, 36(1), pp.103–116.

Herboso, L. et al., 2015. Ecdysone promotes growth of imaginal discs through the regulation of Thor in D. melanogaster. *Scientific Reports*, 5(1), p.12383.

Honegger, B. et al., 2008. Imp-L2, a putative homolog of vertebrate IGF-binding protein 7, counteracts insulin signaling in Drosophila and is essential for starvation resistance. *Journal of biology*, 7(3), p.10.

Huang, J. et al., 2009. Directed, efficient, and versatile modifications of the Drosophila genome by genomic engineering. *Proceedings of the National Academy of Sciences*, 106(20), pp.8284–8289.

Jaiswal, M., Agrawal, N. & Sinha, P., 2006. Fat and Wingless signaling oppositely regulate epithelial cell-cell adhesion and distal wing development in Drosophila. *Development (Cambridge, England)*, 133(5), pp.925–935.

Jones, E., Oliphant, T. & Peterson, P., 2001. SciPy: Open Source Scientific Tools for Python. Available at: http://www.scipy.org/.

Kim, D. et al., 2013. TopHat2: accurate alignment of transcriptomes in the presence of

insertions, deletions and gene fusions. *Genome Biology*, 14(4), p.R36.

Kozlova, T. & Thummel, C.S., 2000. Steroid regulation of postembryonic development and reproduction in drosophila. *Trends in Endocrinology and Metabolism*, 11(7), pp.276–280.

Lavrynenko, O. et al., 2015. The ecdysteroidome of Drosophila: influence of diet and development. *Development*, 142(21).

Legoff, L. et al., 2013. A global pattern of mechanical stress polarizes cell divisions and cell shape in the growing Drosophila wing disc. *Development (Cambridge, England)*, 140(19), pp.4051–9.

Li, L. et al., 2010. Nutritional control of gene expression in Drosophila larvae via TOR, Myc and a novel cis-regulatory element. *BMC Cell Biology*, 11(1), p.7.

Mao, Y. et al., 2006. Dachs: an unconventional myosin that functions downstream of Fat to regulate growth, affinity and gene expression in Drosophila. *Development (Cambridge, England)*, 133(13), pp.2539–51.

Mao, Y. et al., 2013. Differential proliferation rates generate patterns of mechanical tension that orient tissue growth. *The EMBO Journal*, 32(21), pp.2790–2803.

Mao, Y. et al., 2011. Planar polarization of the atypical myosin Dachs orients cell divisions in Drosophila. *Genes & Development*, 25(2), pp.131–136.

Marois, E., Mahmoud, A. & Eaton, S., 2006. The endocytic pathway and formation of the Wingless morphogen gradient. *Development*, 133(2).

Martin, M., 2011. Cutadapt removes adapter sequences from high-throughput sequencing reads. *EMBnet.journal*, 17(1), p.10.

Merkel, M. et al., 2014. The balance of prickle/spiny-legs isoforms controls the amount of coupling between core and fat PCP systems. *Current Biology*, 24(18), pp.2111–2123.

Merkel, M. et al., 2017. Triangles bridge the scales: Quantifying cellular contributions to tissue deformation. *Physical Review E*, 95(3), p.32401.

Micchelli, C.A. & Blair, S.S., 1999. Dorsoventral lineage restriction in wing imaginal discs requires Notch. *Nature*, 401(6752), pp.473–476.

Micchelli, C. a, Rulifson, E.J. & Blair, S.S., 1997. The function and regulation of cut expression on the wing margin of Drosophila: Notch, Wingless and a dominant negative role for Delta and Serrate. *Development (Cambridge, England)*, 124, pp.1485–1495.

Milán, M., Campuzano, S. & García-Bellido, a, 1996. Cell cycling and patterned cell proliferation in the Drosophila wing during metamorphosis. *Proceedings of the National Academy of Sciences of the United States of America*, 93(21), pp.11687–92.

Milner, M.J., 1977. The eversion and differentiation of Drosophila melanogaster leg and wing imaginal discs cultured in vitro with an optimal concentration of β-ecdysone. *Development*, 37(1).

Mirth, C.K., Truman, J.W. & Riddiford, L.M., 2009. The ecdysone receptor controls the post-critical weight switch to nutrition-independent differentiation in Drosophila wing imaginal discs. *Development (Cambridge, England)*, 136(14), pp.2345–53.

Mitchell, N.C. et al., 2013. The Ecdysone receptor constrains wingless expression to pattern cell cycle across the Drosophila wing margin in a cyclin B-dependent manner. *BMC Developmental Biology*, 13(1), p.28.

Okamoto, N. et al., 2013. A secreted decoy of InR antagonizes insulin/IGF signaling to restrict body growth in drosophila. *Genes and Development*, 27(1), pp.87–97.

Ono, H. et al., 2006. Spook and Spookier code for stage-specific components of the ecdysone biosynthetic pathway in Diptera. *Developmental Biology*, 298(2), pp.555–570.

Pastor-Pareja, J.C. & Xu, T., 2011. Shaping Cells and Organs in Drosophila by Opposing Roles of Fat Body-Secreted Collagen IV and Perlecan. *Developmental cell*, 21(2), pp.245–56.

Preibisch, S., Saalfeld, S. & Tomancak, P., 2009. Globally optimal stitching of tiled 3D microscopic image acquisitions. *Bioinformatics (Oxford, England)*, 25(11), pp.1463–5.

Puig, O. et al., 2003. Control of cell number by Drosophila FOXO: downstream and feedback regulation of the insulin receptor pathway. *Genes & development*, 17(16), pp.2006–20.

Resino, J., Salama-Cohen, P. & García-Bellido, A., 2002. Determining the role of patterned cell proliferation in the shape and size of the Drosophila wing. *Proceedings of the National Academy of Sciences of the United States of America*, 99(11), pp.7502–7.

Rogulja, D., Rauskolb, C. & Irvine, K.D., 2008. Morphogen Control of Wing Growth through the Fat Signaling Pathway. *Developmental Cell*, 15(2), pp.309–321.

Rulifson, E.J. et al., 1996. wingless refines its own expression domian on the Drosophila wing margin. *Nature*, 384(6604), pp.72–4.

Rulifson, E.J., Kim, S.K. & Nusse, R., 2002. Ablation of Insulin-Producing Neurons in Flies: Growth and Diabetic Phenotypes. *Science*, 296(5570).

Sagner, A. et al., 2012. Establishment of global patterns of planar polarity during growth of the drosophila wing epithelium. *Current Biology*, 22(14), pp.1296–1301.

Schindelin, J. et al., 2012. Fiji: an open-source platform for biological-image analysis. *Nature methods*, 9(7), pp.676–82.

Schwank, G. et al., 2011. Antagonistic growth regulation by Dpp and Fat drives uniform cell proliferation. *Developmental cell*, 20(1), pp.123–30.

Spellberg, M.J., Marr, M.T. & II, 2015. FOXO regulates RNA interference in Drosophila and protects from RNA virus infection. *Proceedings of the National Academy of Sciences of the United States of America*, 112(47), pp.14587–92.

Teleman, A.A. et al., 2008. Nutritional Control of Protein Biosynthetic Capacity by Insulin via Myc in Drosophila. *Cell Metabolism*, 7(1), pp.21–32.

Trapnell, C. et al., 2012. Differential gene and transcript expression analysis of RNA-seq experiments with TopHat and Cufflinks. *Nature Protocols*, 7(3), pp.562–578.

Tsao, C.-K. et al., 2016. Long Term Ex Vivo Culture and Live Imaging of Drosophila Larval Imaginal Discs A. Bergmann, ed. *PLOS ONE*, 11(9), p.e0163744.

Waddington, C.H., 1940. The genetic control of wing development in Drosophila. *Journal of Genetics*, 41, pp.75–139.

Worley, M.I., Setiawan, L. & Hariharan, I.K., 2013. TIE-DYE: a combinatorial marking system to visualize and genetically manipulate clones during development in Drosophila melanogaster. *Development*, 140(15).

Wu, X. & Chen, D.Z., 2002. Optimal Net Surface Problems with Applications. In Springer, Berlin, Heidelberg, pp. 1029–1042.

Yan, D. & Lin, X., 2009. Shaping morphogen gradients by proteoglycans. *Cold Spring Harbor perspectives in biology*, 1(3).

Yoshiyama, T. et al., 2006. Neverland is an evolutionarily conserved Rieske-domain protein that is essential for ecdysone synthesis and insect growth. *Development*, 133(13).

Yu, G. et al., 2012. clusterProfiler: an R Package for Comparing Biological Themes Among Gene Clusters. *OMICS: A Journal of Integrative Biology*, 16(5), pp.284–287.

Zartman, J., Restrepo, S. & Basler, K., 2013. A high-throughput template for optimizing Drosophila organ culture with response-surface methods. *Development*, 140(3).

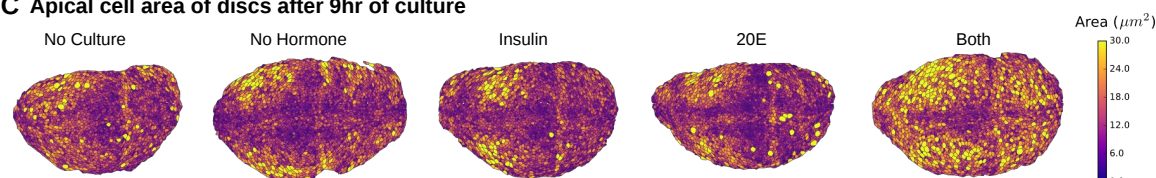## Figure 1: 20E is sufficient to stimulate prolonged cell division in cultured wing discs

A Mitotic cells remaining after culture
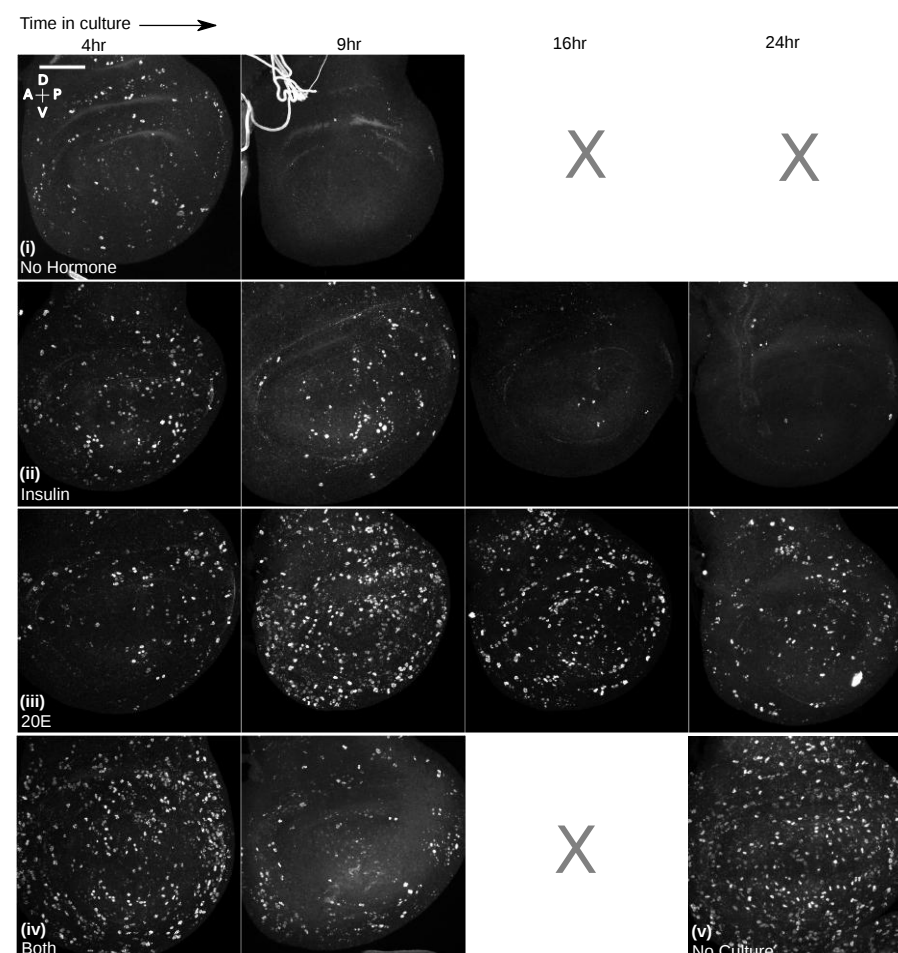
B Quantification of mitotic cell density
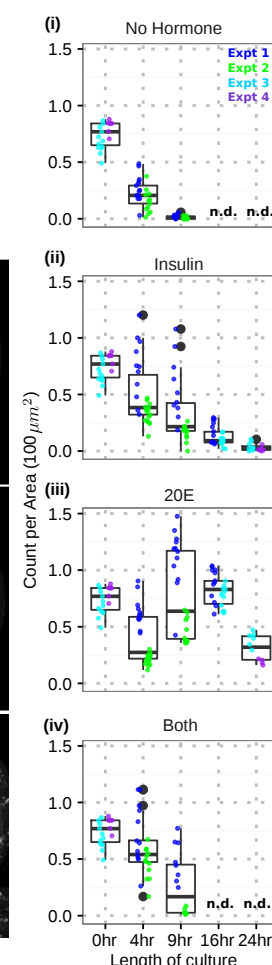
**C** Apical cell area of discs after 9hr of culture

Wing discs from mid-third instar larvae (96hr AEL) were cultured for indicated times and then stained with phospho-Histone H3 to detect mitotic nuclei at the indicated timepoints. (A) Representative images and (B) their quantification. Scale bar indicates 50um. Discs were given (i) no hormone supplement, (ii) 5ug/ml insulin, (iii) 20nM 20E or (iv) both. In (v) is an image of an uncultured disc from the beginning of the experiment (96hr AEL). In (B), we show pooled results from multiple experiments from different days. Each dot is the mean density of mitotic nuclei (# nuclei per 10x10um2 area, averaged across the pouch from a single disc). Discs from experiments performed on the same day have the same color. The box plots summarize all data for each condition. Hinges correspond to the first and third quartiles; lines extend to the highest and lowest values within 1.5*IQR (inter-quartile range); outlier points are black. n.d. = not determined. (C) Apical cell area the wing pouch after 9hr of culture. Overall, the morphology is maintained during culture, except in presence of both hormones. Lowering the concentration of 20E in combination with insulin does not further prolong proliferation (See Fig. 1--Figure Supplement 1).

**Figure 2: Size and overlap of the transcriptional response to 20E or insulin**
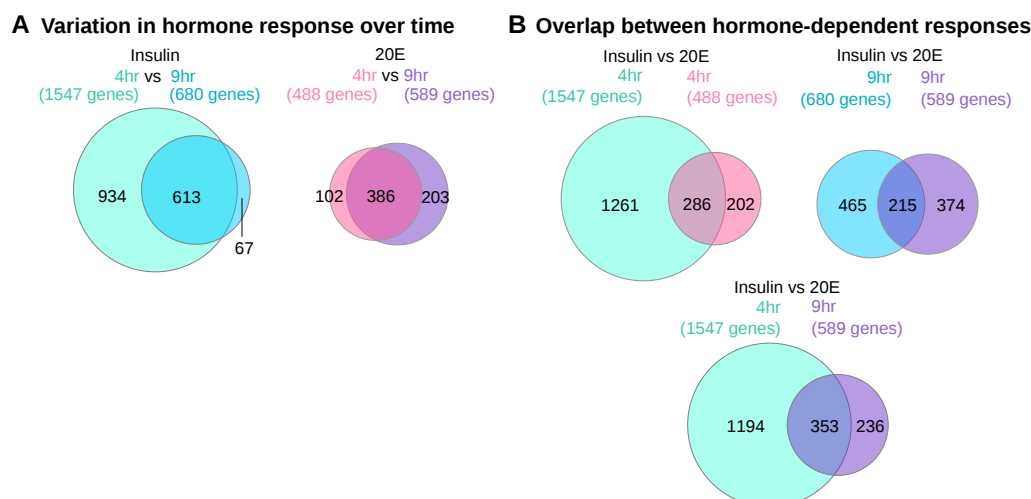
Transcriptomes of wing discs cultured in either 20E or insulin were sequenced and compared to those of uncultured discs and discs cultured without any hormone. A gene was classified as hormone-dependent if its levels changed upon culture without hormone and responded in the correct direction (more similar to uncultured levels) when cultured with hormone. (A) Total number of genes that responded to 20E or insulin at two timepoints. (B) Overlap between the hormone-dependent responses at 4hr (left), 9hr (right) or when each hormone supports the most amount of proliferation (4hr for insulin, 9hr for 20E). Circles are all drawn to scale. Numbers denote the amount of genes in the overlapping or non-overlapping sets.

Figure 3: Processes that are transcriptionally regulated by insulin in cultured discs
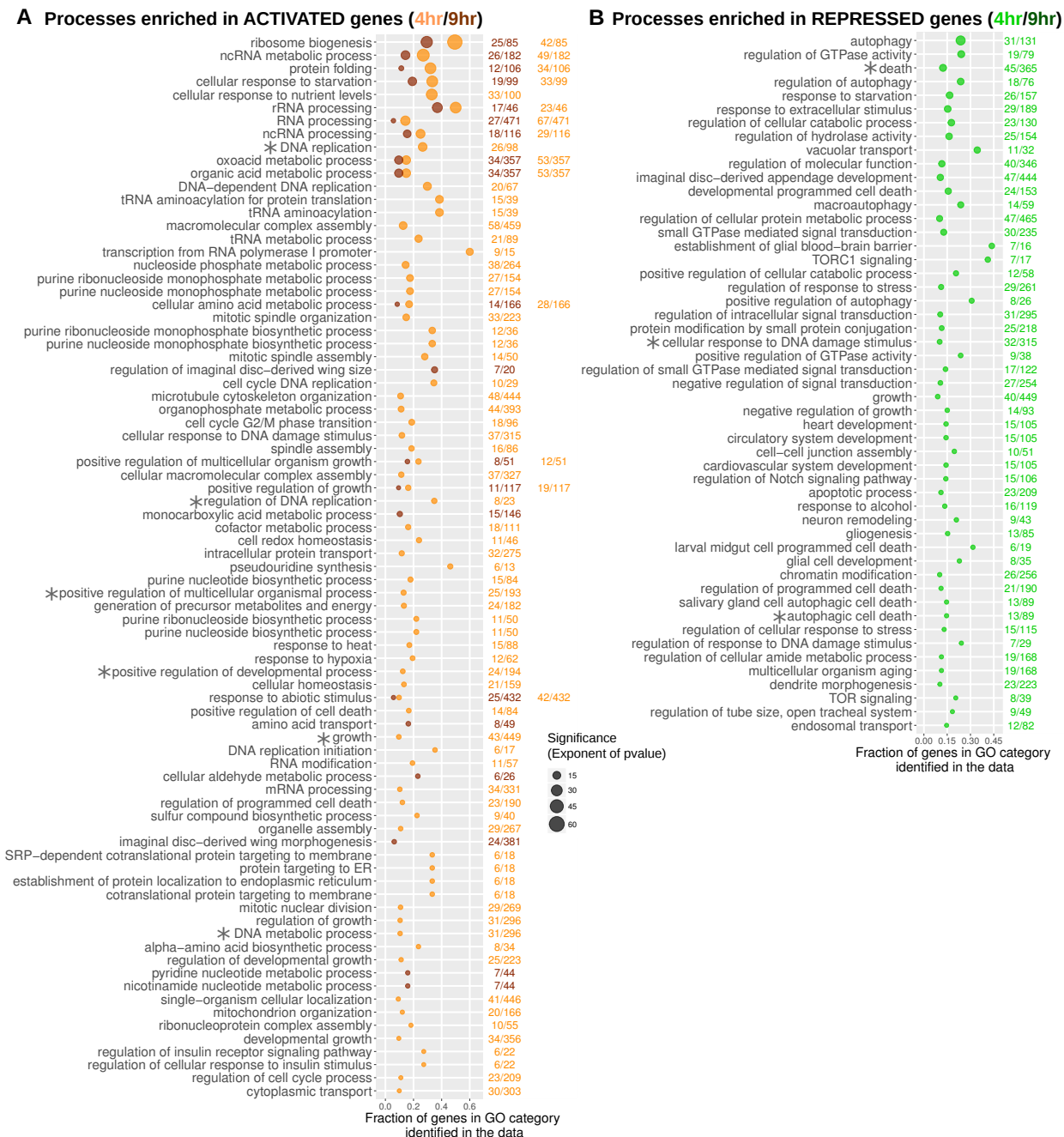
A Processes enriched in ACTIVATED genes (4hr/9hr)

B Processes enriched in REPRESSED genes (4hr/9hr)

Shown are the Biological Process (BP) Gene Ontology (GO) terms that are significantly enriched in the set of genes identified to be activated (A) or repressed (B) by insulin in cultured wing discs (simplified with a semantic similarity algorithm; threshold=0.95). In both (A) and (B), we plot the GO terms according to the fraction of its total genes that were identified in the data (# genes in the data with this GO term/total size of the GO term). The size of the point indicates the significance of enrichment (BH-corrected p-value; cutoff of p <0.005). The color indicates either 4hr (light orange in A, green in B) or 9hr of culture (dark orange in A, dark green in B). Note that by 9hr of culture in insulin, no GO terms are enriched in the group of genes repressed by insulin (B). Asterisks indicate terms shared by both insulin and 20E. Note that many categories are only enriched (or more significantly enriched) at 4hr. This transience in the response to insulin must result from downregulation of the pathway at a point downstream of PI3K activation, since a fluorescent reporter of this enzyme's activity indicates that it is still active for the duration of culture (See Fig 3--Figure Supplement 2).

Figure 4: Processes that are transcriptionally regulated by 20E in cultured discs
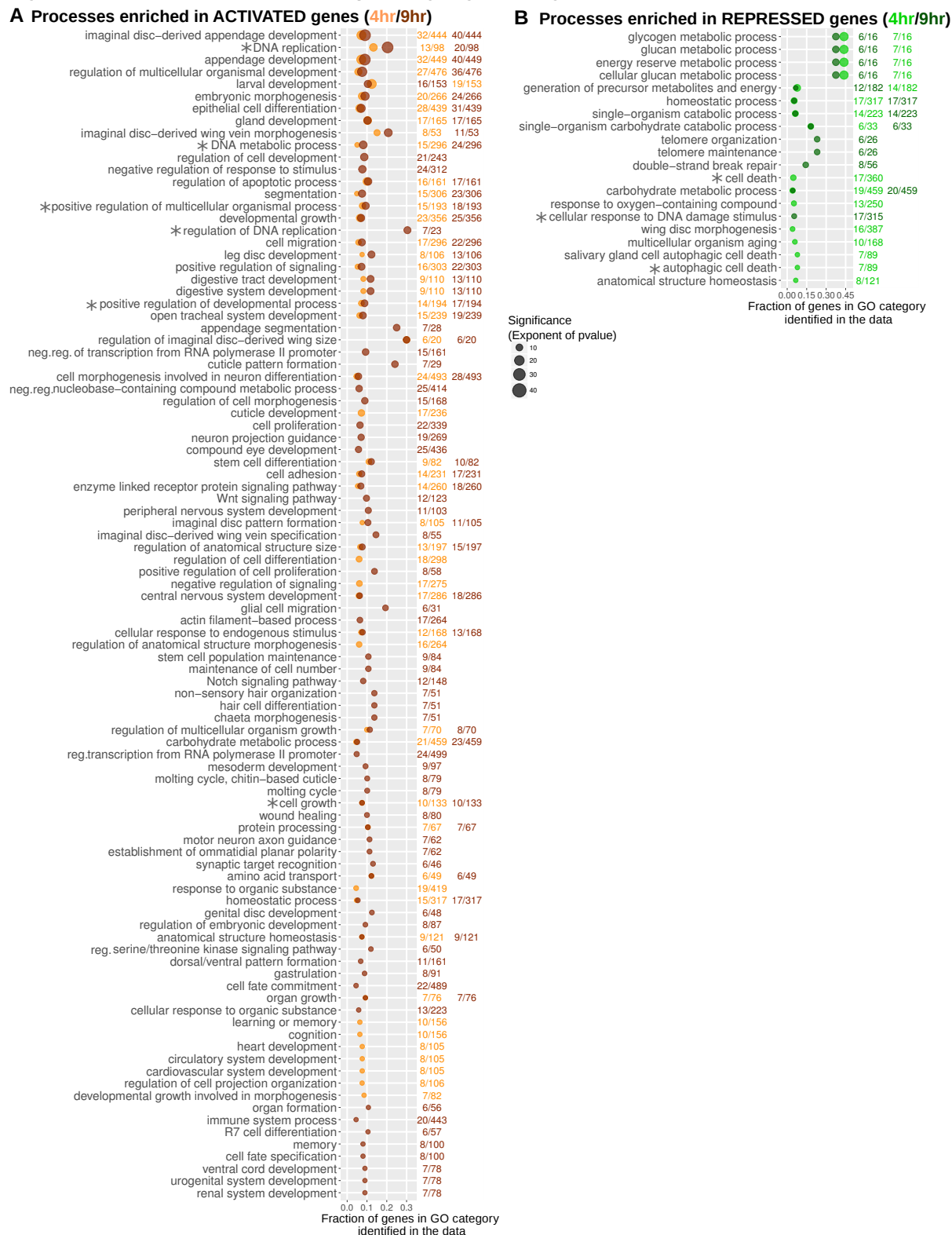
A Processes enriched in ACTIVATED genes (4hr/9hr)   **B** Processes enriched in REPRESSED genes (4hr/9hr)

Shown are the Biological Process (BP) Gene Ontology (GO) terms that are significantly enriched in the set of genes identified to be activated (A) or repressed (B) by 20E in cultured wing discs (simplified with a semantic similarity algorithm; threshold=0.9). In both (A) and (B), we plot the GO terms according to the fraction of its total genes that were identified in the data (# genes in the data with this GO term/total size of the GO term). The size of the point indicates the significance of enrichment (BH-corrected p-value; cutoff of p <0.005). The color indicates either 4hr (light orange in A, green in B) or 9hr of culture (dark orange in A, dark green in B). Asterisks indicate terms shared by both insulin and 20E.

Figure 5: Patterning and morphogenesis genes that are regulated by 20E in culture
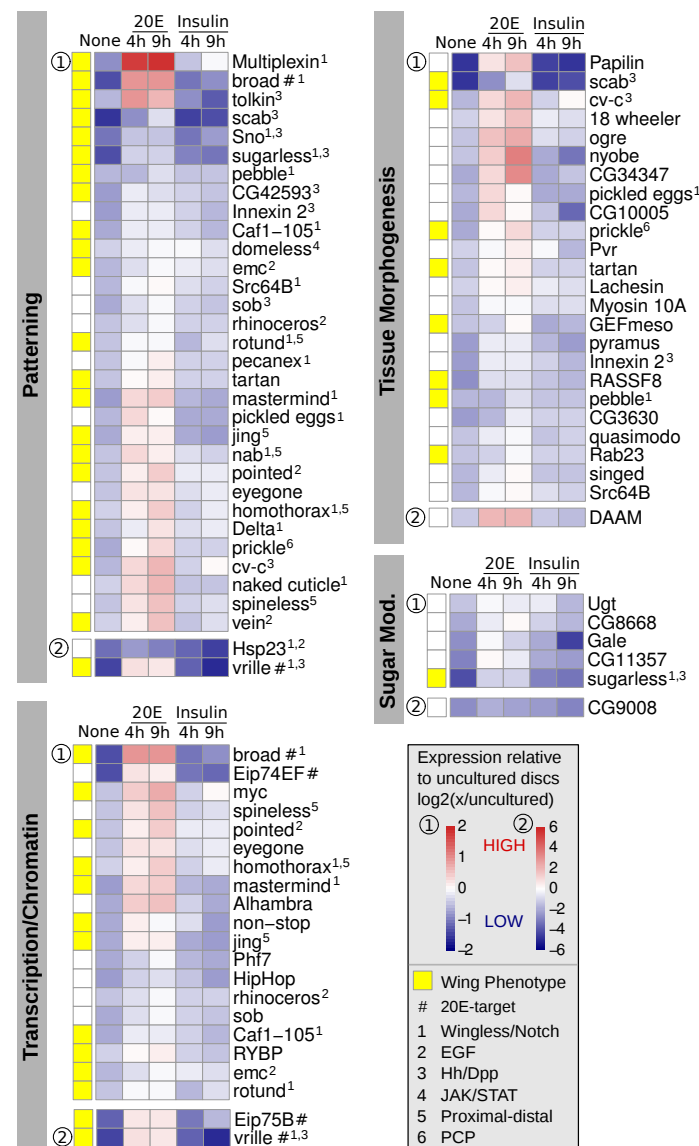
Normalized expression values are plotted across all conditions for selected 20E-regulated genes. The expression value of each gene (fkpm) is shown relative to its expression in uncultured discs, log2(x/uncultured). Genes were plotted on one of two scales (labeled as 1 or 2), depending on how much its values changed across conditions. Yellow squares indicate genes with published loss-of-function phenotypes in the wing. Previously identified 20E-targets and genes with known connections to specific patterning systems (in any context) are indicated.

Figure 6: Widespread effects on morphogen signaling and PCP upon perturbation of 20E signaling *in vivo*

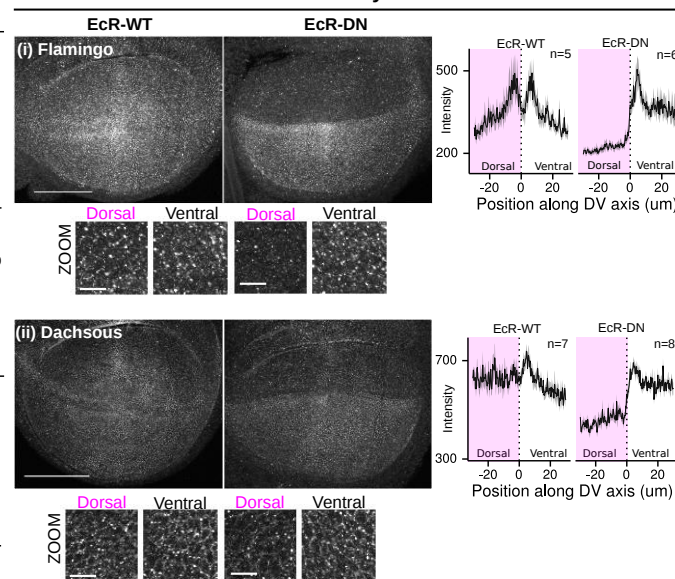**A** Quantification of effect of dorsal EcR-DN overexpression on spatial patterns of gene expressionn
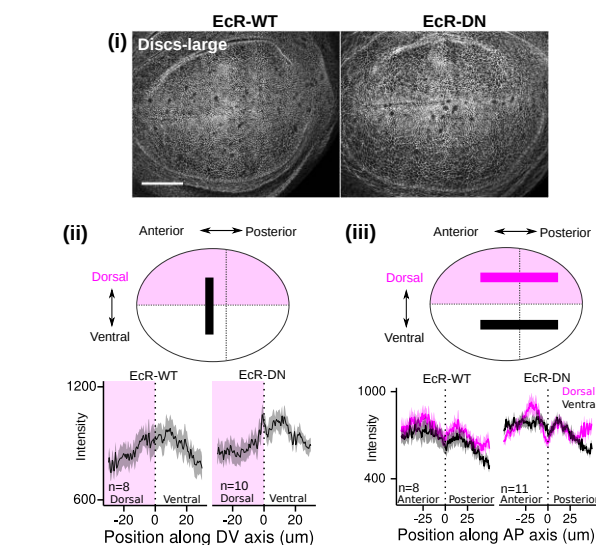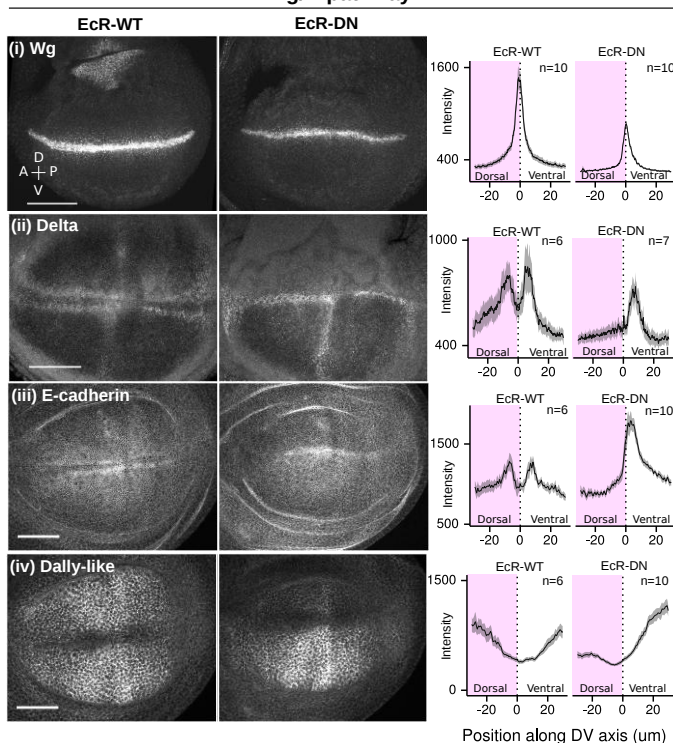
C Hh/Dpp pathway

B Wg/N pathway
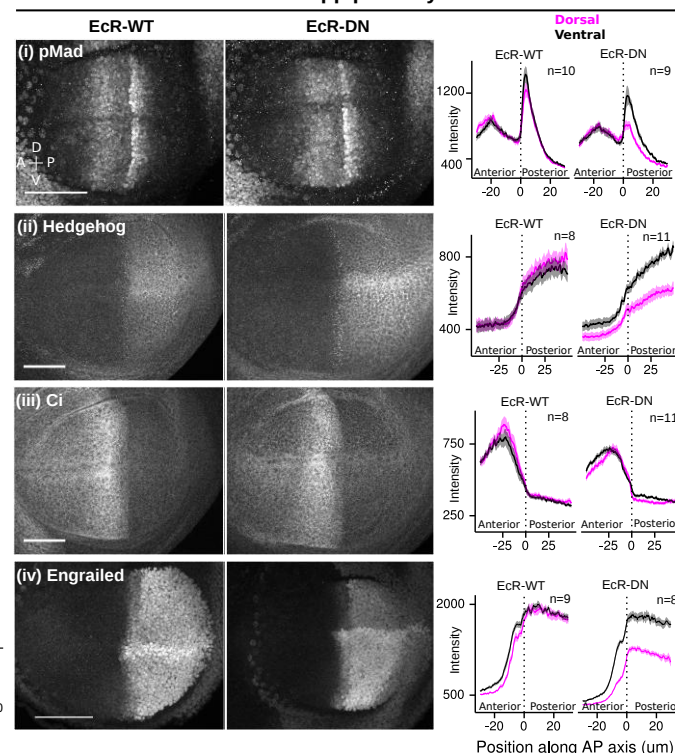
D Polarity

A dominant-negative allele of EcR-B1 (W650A, abbreviated EcR-DN) was overexpressed for 24hr in the dorsal compartment of the wing pouch using apterous-GAL4 and temperature-sensitive GAL80. As a negative control performed in parallel, we overexpressed the wild type EcR-B1 gene (EcR-WT), which does not significantly affect growth or proliferation of the disc (Fig. 6--Figure Supplement 1) (A). Quantification of the expression patterns in this experiment was done in one of two ways, each demonstrated in (A) for Discs-large (i), a septate junction marker. The first scheme (Aii) was used for proteins in (B) and (D): the intensity profile (arbitrary units) along a line in the Anterior compartment, drawn from Dorsal to Ventral, was compared between EcR-WT and EcR-DN expressing discs. For Discs-large (Aii), this profile is unaffected by EcR-DN expression. In contrast, intensity in the dorsal (pink shaded) compartments is altered for the morphogen Wg (Bi), the Notch ligand Delta (Bii), adhesion protein E-Cadherin (Biii), the HSPG Dallylike (Biv), the core PCP component Flamingo (Di) and the Fat PCP component Dachsous (Dii). The lower images of parts Di-ii are zoomed-in regions from the anterior compartment of the above images. The effect on the stripe of Wg expression was confirmed by expressing EcR-DN in the posterior compartment (Fig. 6--Figure Supplement 2). The second scheme (Aiii) was used for the Hh/Dpp pathways (C): the profile of absolute intensity along a line drawn from Anterior to Posterior in the Dorsal compartment (pink) was compared to that along a line drawn in the Ventral compartment (black). For Discs-large (Aiii), the black and pink lines are similar, both in EcR-WT (left) and EcR-DN (right) expressing discs. However, a readout of Dpp signaling, pMAD (Ci) was affected, particularly in the posterior compartment, by EcR-DN expression. In addition, compartment-autonomous differences in the Hh pathway were observed: at the level of Hh itself (Cii), its transcriptional coactivator Ci (Ciii), and the downstream target Engrailed (Civ). The effect of perturbing 20E signaling on Wg, Hh, Ci, Engrailed, and Discs-large were confirmed by an independent method (removal of circulating 20E) in Fig. 6--Figure Supplement 3. Scale bars for the zoomed regions in D are 20um; elsewhere they are 50um. In all quantified intensity profiles, the solid line represents the mean of several discs from the same experiment (precise # depicted in each graph), and the shaded ribbon is the standard deviation. All images are shown with dorsal up and anterior to the left.
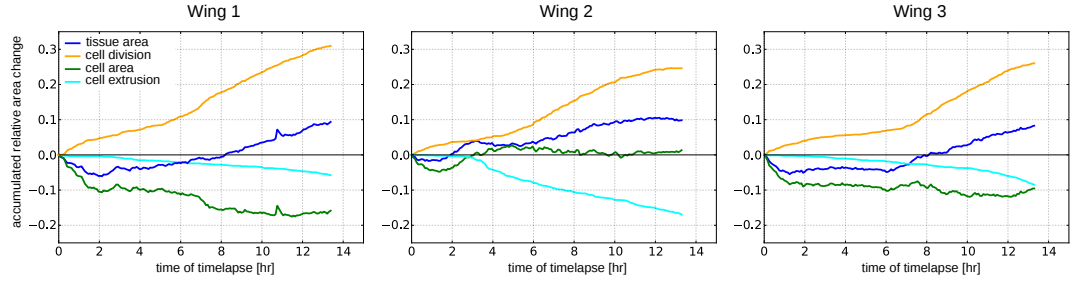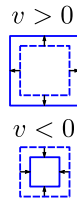
Figure 7: Quantification of tissue growth and its cellular contributions
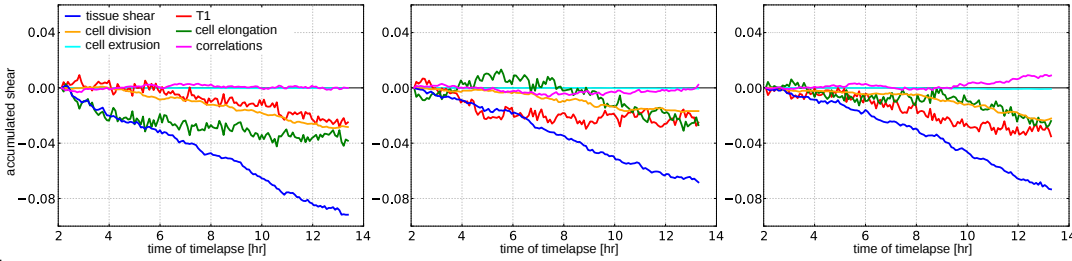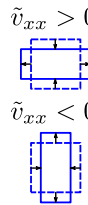
A Tissue shear flow pattern
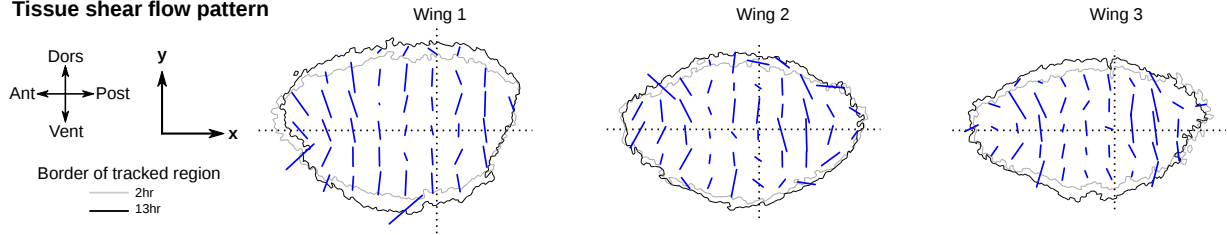
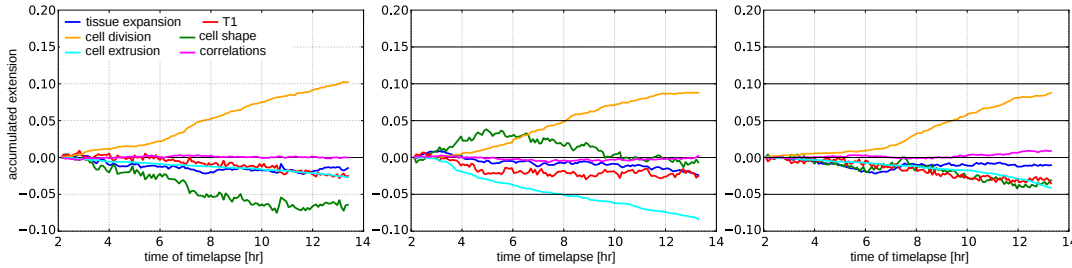**B** Cellular contributions to accumulated tissue area and shape changes
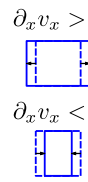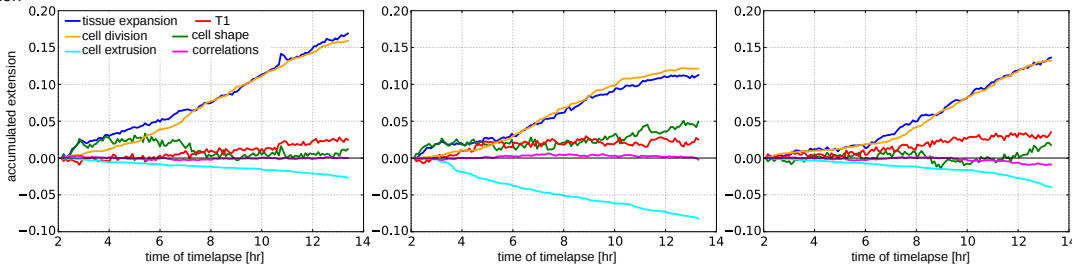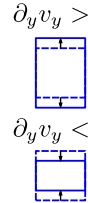

Three E-Cadherin-GFP-expressing wing discs were imaged for >13hr, and cells in the future wing blade region were segmented and tracked. (A) Tissue shear was accumulated between 2hr and 13hr in local regions of the tissue defined by a grid. Accumulated shear is represented by blue bars plotted on outlines of the tracked region at 2hr (grey) and 13hr (black). (B) The trace of the velocity gradient tensor $v = \partial_x v_x + \partial_y v_y$ quantifies the relative change of tissue area. The diagonal component of the traceless symmetric part of the velocity gradient tensor $\tilde{v}_{xx} = (\partial_x v_x + \partial_y v_y)/2$ quantifies the tissue shear flow along x- and y-axes. (i) Relative change of tissue area, accumulated from the start of the timelapse, contains contributions from average cell area change, cell divisions and cell extrusions. In all experiments, positive tissue area growth (blue) is driven by cell divisions (orange) and partially opposed by cell extrusions (cyan) and cell area change (green). (ii) Accumulated tissue shear along the x-axis, averaged over the entire tracked region is plotted as a function of time (blue). The continuous shear of the blade perpendicular to the x-axis (negative values of blue curve) is composed of similar contributions from cell elongation change (green), T1 transitions (red) and cell divisions (orange). Contributions from cell extrusions (cyan) and correlations (magenta) are negligible. (iii-iv) Velocity gradient components, $\partial_x v_x$ and $\partial_y v_y$ represent tissue extension or compression along the x- and y-axis, respectively. We calculated the accumulated extensions along x- and y-axes from the relative area change of the tissue and the tissue shear. Cellular contributions to the tissue expansion along the x-axis were determined as described in the Methods. We find that the tissue does not extend along the x axis (blue line in iii), although cell divisions do contribute to tissue expansion along x axis (orange line in iii). In contrast, tissue extension along y axis (blue line in iv) closely follows the cell division contribution (orange line in iv). The sum of other contributions is small.

Figure 1--Figure Supplement 1:
Effect of insulin on proliferation is not improved by lower 20E concentration
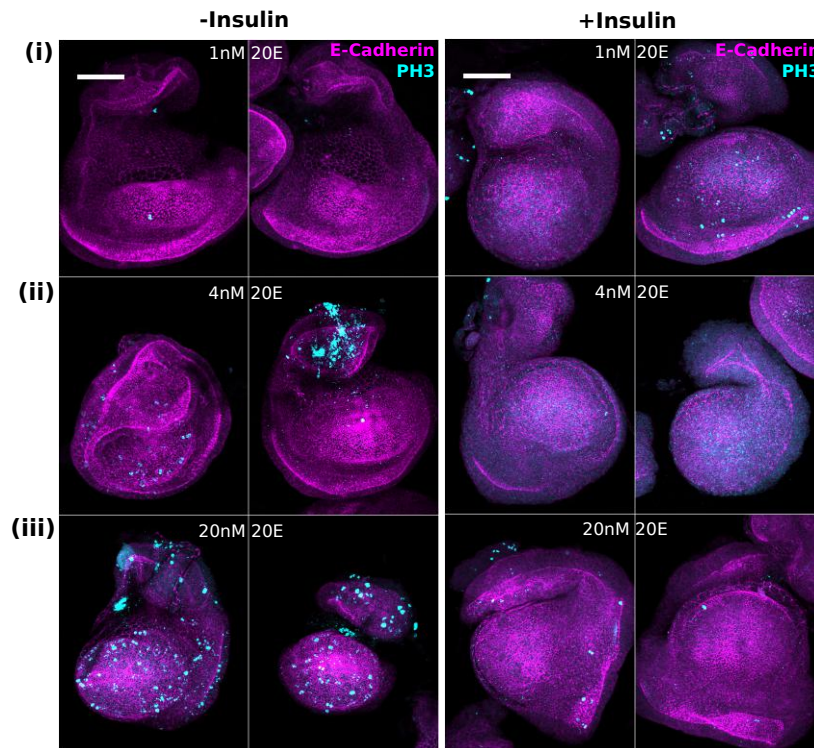
To determine if lower concentrations of 20E would allow insulin to further improve proliferation, discs were cultured for 24hr in 1nM (**i**), 4nM (**ii**) or 20nM (**iii**) 20E, with or without 5ug/ml insulin (right/left, respectively). After this length of culture, discs start to lose their morphology, making quantification difficult. In particular in insulin (+/- 20E), the pouch region balloons forward and out. In all discs, the prospective notum starts to curl forward. Only in 20nM 20E alone (without insulin) is there any consistent division remaining. Best attempts were made to orient images with anterior to the left and dorsal up. Scale bar is 50um.

Figure 3--Figure Supplement 1:
Cellular component GO terms enriched in insulin-regulated geneset

A Localizations enriched in ACTIVATED at 4hr/9hr
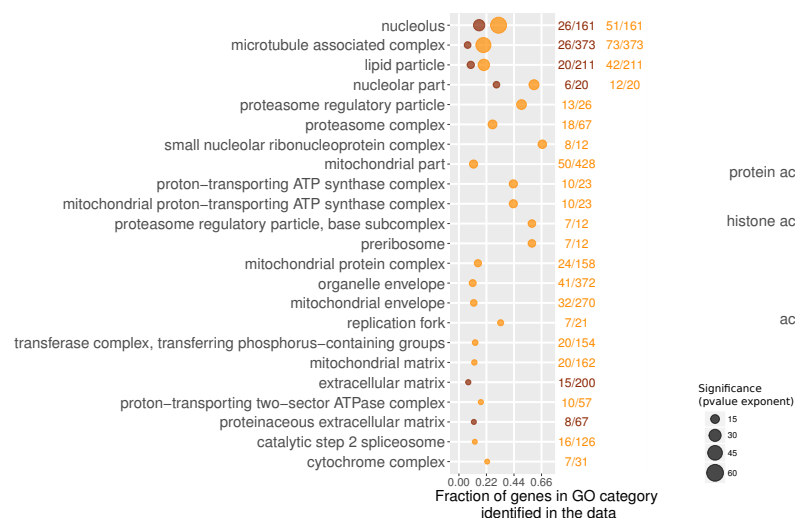
B Localizations enriched in REPRESSED at 4hr/9hr
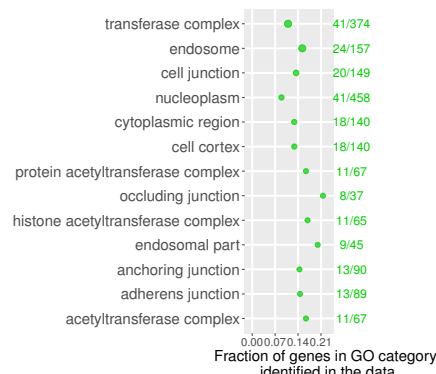
C Normalized expression levels of a genes in enriched cellular component GO terms
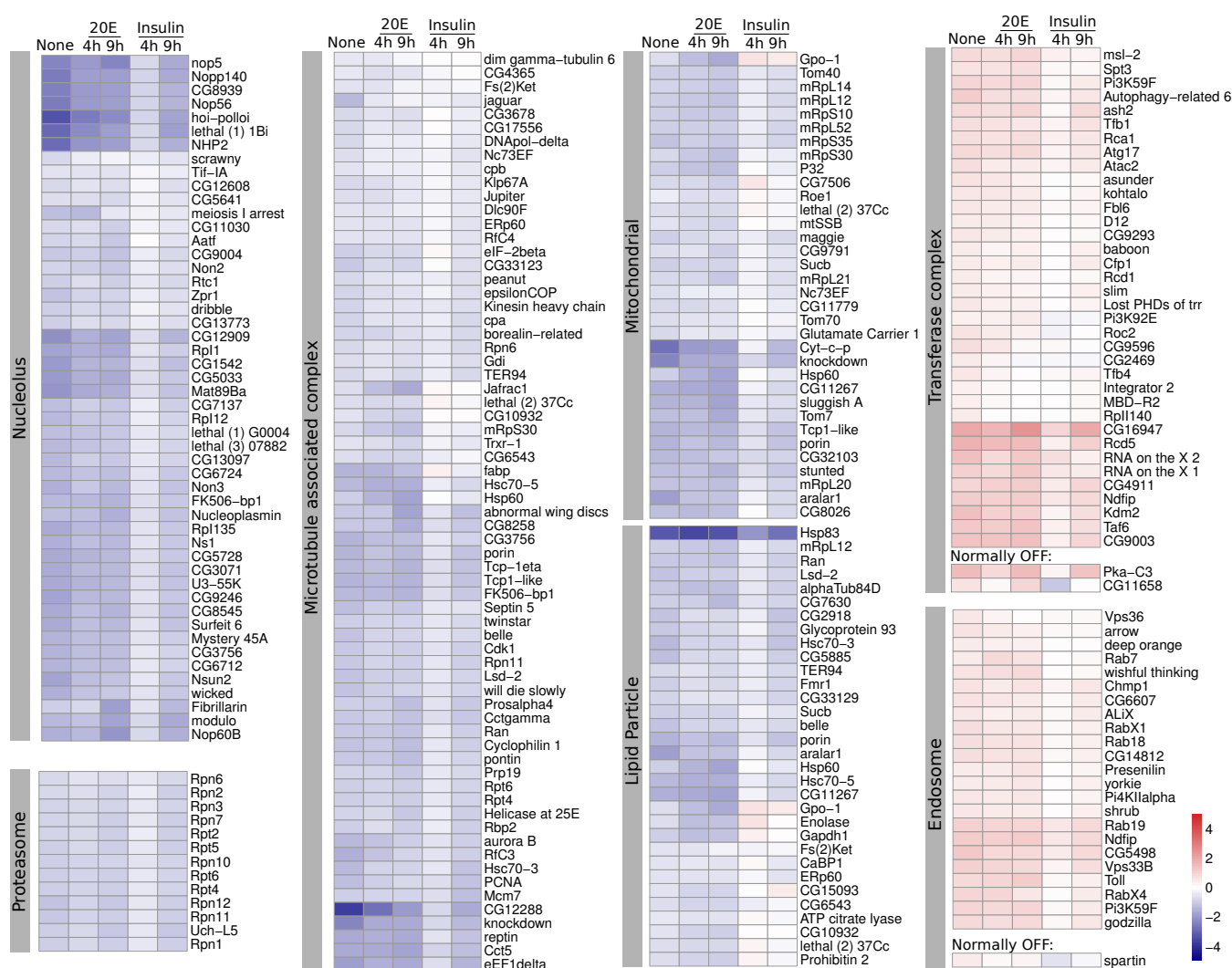
The insulin-regulated genes were analyzed as in Fig. 3 but using the Cellular Component (CC) terms. In both **A** and **B**, the fraction of total genes in the GO category represented in the dataset is plotted along x, with the actual numbers written on the right. The size of the point indicates the significance of enrichment (BH-corrected p-value). The cutoff for enrichment was a p-value <0.005. The color indicates the number of genes in that group at either 4hr of culture (light orange in **A**, green in **B**) or 9hr of culture (dark orange in **A**, dark green in **B**). (**C**) The expression of selected genes (fpkm) in related CC-enriched GO categories is shown for all of the tested conditions, normalized to its levels in uncultured wing discs (log 2(x/uncultured)). In rare cases when a gene was ectopically activated (expression in culture but not in uncultured discs, labeled as "normally OFF"), its levels were normalized to the threshold for expression (5fpkm).

Figure 3--Figure Supplement 2:
PI3K activity reporter remains active during long term culture in insulin

A PH-GFP reporter of PI3K activity during culture with insulin alone
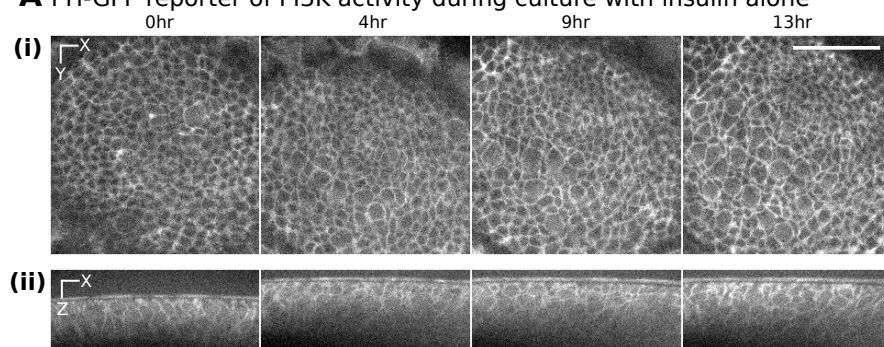
B PH-GFP reporter of PI3K activity during culture without hormone
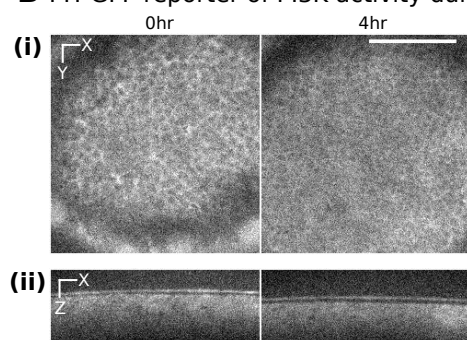
PH-GFP reporter of PI3K activity during culture with insulin **(A)** or no hormone **(B)**. This reporter localizes to the membrane upon PIP3 production, thus reflecting PI3K activity. A single xy plane is shown in **(i)** and an xz slice through the middle of the disc is shown in **(ii)**. Timepoints shown in each part are from the same disc grown on the microscope. Scale bar is 20um.

Figure 4--Figure Supplement 1:
Partial overlap between insulin- and 20E-regulated genesets

A Enriched Biological Process GO terms

| GO term	Fraction
DNA replication	15/98
DNA–dependent DNA replication	12/67
DNA metabolic process	17/296
positive regulation of multicellular organismal process	13/193
positive regulation of developmental process	12/194
growth	19/449
developmental growth	16/356
instar larval development	7/70
regulation of apoptotic process	10/161
regulation of multicellular organismal development	18/476
imaginal disc–derived wing vein morphogenesis	6/53

Fraction of genes in GO category identified in the data

B Enriched Cellular Component GO terms

GO term	Fraction
nucleolus	10/161
endoplasmic reticulum	13/296

Fraction of genes in GO category identified in the data

Count
- 10
- 20

Significance (pvalue exponent)
20 / 15 / 10 / 5

C Normalized expression of selected genes with potential growth regulating functions

DNA replication and Cell Cycle

(i) Both equal
20E / Insulin
None 4h 9h 4h 9h

① string **
sister of feo
CG2990
Ras opposite
Orc2
Ctf4 **
DNApol–alpha60
aurora borealis
PCNA
RfC3
DNApol–alpha73
Rif1
RnrL **
DNApol–eps255 **
RnrS **
CG2865
WRN exonuclease **
Mcm10
DNApol–epsilon58

(ii) Stronger effect of insulin
20E / Insulin
None 4h 9h 4h 9h

① Cyclin B
② lethal (1) 1Bi

Cell Death/DNA damage

(i) Both equal
20E / Insulin
None 4h 9h 4h 9h

① stonewall
klaroid
Tfb4
Ino80
qkr58E–3
Debcl
Tie
rad50
charybde **
scylla **
Lobe
meiotic 41 **

(ii) Stronger effect of insulin
20E / Insulin
None 4h 9h 4h 9h

① CHES–1–like **

Expression relative to that in uncultured discs log2(x/uncultured)
① 2 / ② 6
1 / HIGH
0
–1 / LOW
–2 / –6

* TOR target
** FOXO target
yellow Wing Phenotype

1 Wingless/Notch
2 EGF
3 Hh/Dpp
4 JAK/STAT
5 Proximal-distal
6 PCP

Protein Production

Positive

(i) Both equal
20E / Insulin
None 4h 9h 4h 9h

① SrpRbeta **
Hrb98DE
nonA **
CG7182
CG5885
HIP–R
HIP
Doa **
glorund
CG9107
CG8860

(ii) Stronger effect of insulin
20E / Insulin
None 4h 9h 4h 9h

① Hsc70–3 **
CG2918
CG1542 *
② CG11652 **
hoi–polloi *
Mat89Ba *
CG32409
pitchoune */**
Rbm13 */**
NHP2 *
CG8939 *
Nop56 *
Nopp140 *
krasavietz

(iii) Stronger effect of 20E
20E / Insulin
None 4h 9h 4h 9h

① Pabp2 **
NAT1 **
② Fkbp14 **

Negative

(i) Both equal
20E / Insulin
None 4h 9h 4h 9h

① Tis11 **
qkr58E–3
Dicer–1
Argonaute 2 **
CG4406
Tfb4
mRpL39
fandango **
RpII140
CG7747 **
CG5808
CG9596
② Pdcd4 **
Thor/4E–BP **

Nutrient Transport

(i) Both equal
20E / Insulin
None 4h 9h 4h 9h

① Oatp30B **
Ncc69
Orct2
② CG10960 **

(ii) Stronger effect of insulin
20E / Insulin
None 4h 9h 4h 9h

① CD98 heavy chain
spinster **
② minidiscs
lethal (2) 08717
pathetic

(iii) Stronger effect of 20E
20E / Insulin
None 4h 9h 4h 9h

① CG1607
Glut1

Patterning

(i) Both equal
20E / Insulin
None 4h 9h 4h 9h

① E(spl)mdelta–HLH[1]
Wnt2[1]
dally **[1,3]
net[2]
rhomboid–4[2]
asf1 **[1]
shifted[3]
Transportin[3]
short gastrulation[3]
scarface
string **[1]
drumstick[1,3]
Sorting nexin 3[1]
② tal–2A[1]

(ii) Stronger effect of insulin
20E / Insulin
None 4h 9h 4h 9h

① Cyclin B[1]
Sulfated[1,2,3]
spinster **[3]

(iii) Stronger effect of 20E
20E / Insulin
None 4h 9h 4h 9h

① tolloid[3]
dally–like[1,3]
Dpp target gene[3]
four–jointed[1,6]
wingless[1]
② windbeutel[3]
Fkbp14 **[1]
nemo **[1,3,6]

Enriched biological process (**A**) or cellular component (**B**) GO terms were identified in the set of genes activated by both insulin (at 4hr) and 20E (at 9hr). A semantic similarity algorithm was used to reduce redundancy, with a similarity cutoff of 0.95. Labels on the right indicate the number of genes in the data over total genes in that GO category. (**C**) The expression of genes in selected functional categories (fpkm) is shown for all of the tested conditions, normalized to its levels in uncultured wing discs, log2(x/uncultured). Genes in each group were further subdivided based on whether the two hormones had equal (**i**) or unequal effects (**ii**, insulin stronger vs **iii**, 20E stronger). Genes were plotted on one of two scales (labeled as 1 or 2), depending on how much their values changed across conditions. Yellow squares indicate known phenotypes in the wing (at any stage of development) for loss of function for genes positively regulated by hormone or gain of function for genes negatively regulated by hormone. Asterisks indicate previously identified TOR (*) or FOXO (**) targets. Genes with known patterning functions (in any context) are indicated with numbers.

Figure 6--Figure Supplement 1:
20E-signaling is autonomously required for wing growth during the 3rd instar

A Dorsal overexpression of dominant negative EcR
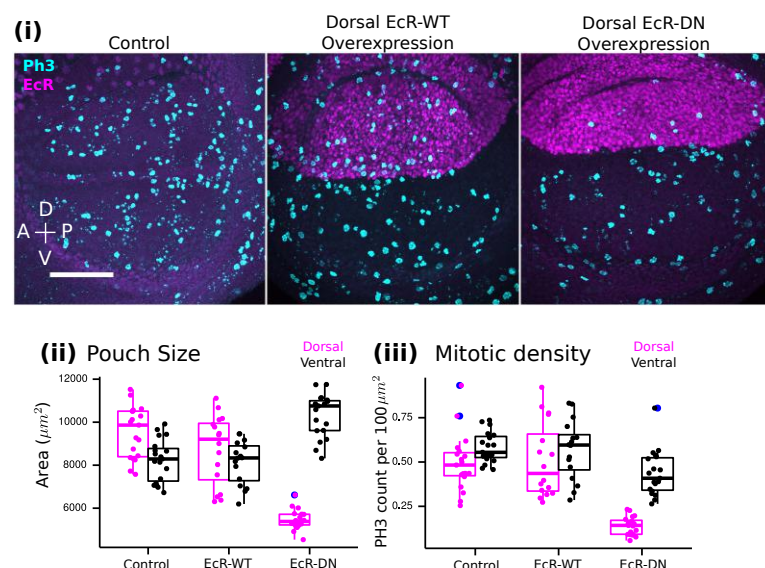
B Removal of circulating 20E
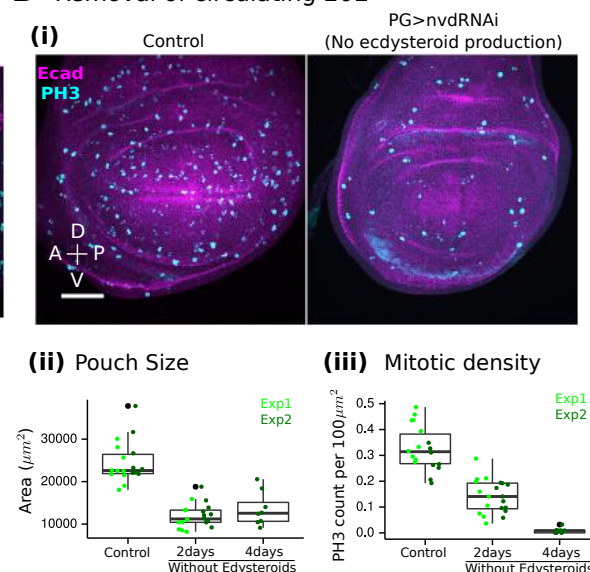
The effect of 20E on larval wing growth was verified by autonomously perturbing 20E signaling by overexpressing a dominant-negative EcR in the dorsal compartment of the wing (**A**) or by genetically preventing the synthesis of 20E (**B**).

A. *Apterous-GAL4*, which is expressed in the dorsal compartment of the wing disc, combined with *tub>GAL80ts* was used to conditionally overexpress either a wild type (EcR-WT) or dominant negative EcR allele (EcRB1-W650A, called EcR-DN). Overexpression of the EcR construct was prevented in early developmental stages by growing the larvae at 18C, and then switching to 29C for 24hr during the third instar. The negative control is the *apterous-GAL4, gal80ts* crossed to wild type (left). Additionally, we verified that overexpression of wild type EcR (B1 isoform) would not affect growth (middle). (**ii**) Pouch size was quantified by measuring area in a maximum projection image. The Dorsal (pink) and Ventral (black) comparments were separately measured, estimating the boundary using E-Cadherin labeling. (**iii**) Density of PH3 staining in the Dorsal (pink) and Ventral (black) compartments.

B *Phantom-GAL4*, which is expressed in the prothoracic ecdysteroid-producing gland of the brain (PG), combined with *tub>GAL80ts* was used to induce an RNAi targeting *neverland* (*nvd*), a gene required to synthesize ecdysone. Induction of the RNAi was prevented in early developmental stages by growing the larvae at 18C, and then switching to 29C at the third instar. Control larvae contained only the *phantom-GAL4, tub>GAL80ts* crossed to wild type, and formed pupae after 2 days at 29C, whereas nvd-RNAi larvae stayed as larvae for several days. Disc size (area in a maximum projection image, **ii**) and density of mitotic nuclei (marked by phospho-histone H3, PH3, **iii**) were measured in the pouch region, defined as the region surrounded by the innermost folds. Data from two independent replicates of the experiment are separately colored. Only pupae remained for the control after 2 days at 29C; thus, only the 4-day timepoint is shown.

For both **A** and **B**: (**i**) representative images show PH3 staining (cyan) as a maximum projection overlaid with either E-Cadherin (**A**) or EcR (**B**) in magenta. Dorsal is up and Anterior to the left. Scale bar is 50um. In (**ii**) and (**iii**), each dot represents one disc, with bars showing the extent of the first and third quartiles; lines reach up to 1.5* IQR (interquartile range); outliers outside of this range are blue (left) or black (right) dots.

Figure 6--Figure Supplement 2:
20E-signaling is required in the posterior compartment for Wg expression
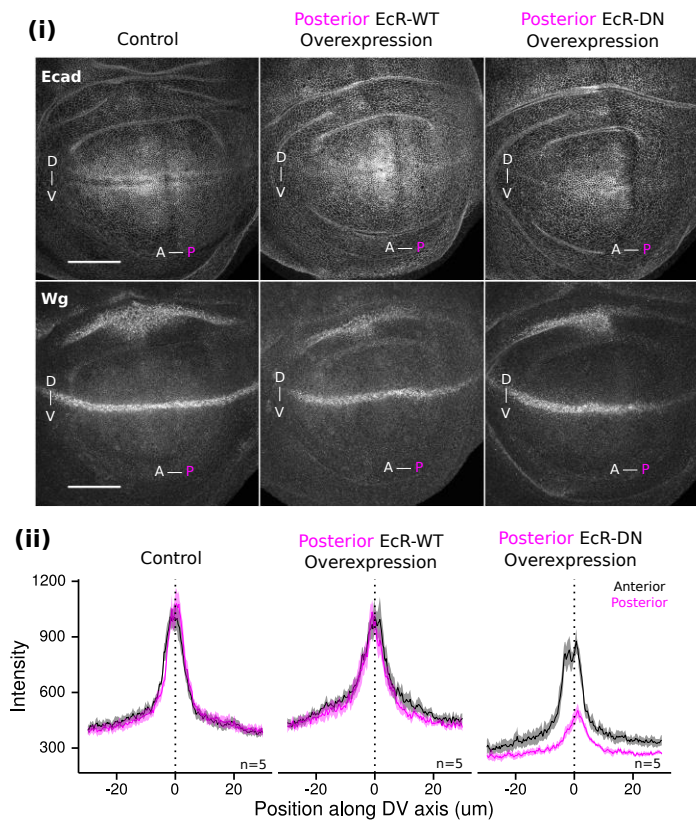
The autonomous effect of 20E-signaling on Wg expression was verified using by overexpressing EcR-DN (EcRB1-W650A) in the posterior compartment. *Engrailed-GAL4*, which is active in the posterior wing disc, was combined with *tub>GAL80ts* to limit expression of the transgenes to 24hr in the third instar using a temperature shift. The control (left) was *engrailed-GAL4, GAL80ts* crossed to wild type flies. Additionally, it was verified that overexpression of a wild type EcR (EcRB1 isoform) did not affect Wg expression (middle) (**i**) Representative images of E-Cadherin (top) or Wg (bottom) staining in the same discs. Dorsal is up, anterior to the left. Markers deliniate the boundaries. Scale bars are 50um. (**ii**) Wg expression was quantified by measuring the absolute intensity alone a line drawn from Dorsal to Ventral of the pouch in the Anterior (black) or Posterior (pink) compartments. Posterior overexpression of EcR-DN (right) but not EcR-WT (middle) affects the Wg gradient. Control and perturbation stainings were done in parallel and imaged with the same acquisition settings on the same day.

Figure 6--Figure Supplement 3:
Circulating ecdysone is required for wing pattern during growth
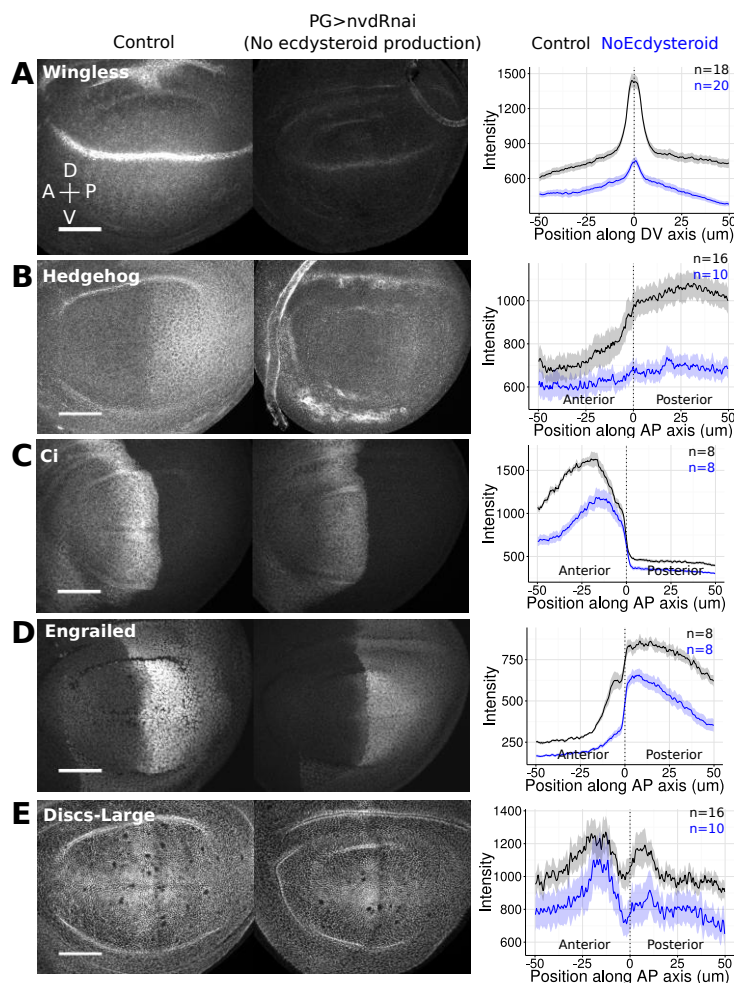
Phantom-GAL4, which is expressed in the prothoracic ecdysteroid-producing gland of the brain (PG), combined with *tub>GAL80TS* was used to induce RNAi against *neverland* (nvd), a gene required to synthesize ecdysone, only during the third larval instar. Expression of Wingless (**A**), Hedgehog (**B**), Ci, the transcriptional activator downstream of Hh signaling (**C**), Engrailed, a Hh target gene (**D**), and Discs-large, a septate junction marker (**E**) was analyzed by immunofluorescence. Quantification of the changes in expression was performed by plotting the absolute intensity along a line drawn from one compartment to another. For (**A**), the line was drawn from Dorsal to Ventral in the Anterior comparment. For (**B**)-(**E**), the line was drawn from Anterior to Posterior in the Dorsal compartment. Black is the control; blue is the nvd-RNAi animals. The dark line is the mean for all discs measured in the same staining experiment; the shaded ribbon indicates the standard deviation. Control and perturbation stainings were done in parallel and imaged with the same acquisition settings on the same day. Scale bars correspond to 50um.